Dielectric spectroscopy of glassy dynamics

Peter Lunkenheimer, Melanie Köhler, Stefan Kastner, Alois Loidl

Angaben zur Veröffentlichung / Publication details:

Lunkenheimer, Peter, Melanie Köhler, Stefan Kastner, and Alois Loidl. 2012. "Dielectric spectroscopy of glassy dynamics." In *Structural glasses and supercooled liquids: theory, experiment, and applications*, edited by Peter G. Wolynes and Vassiliy Lubchenko, 115–49. Hoboken, NJ: John Wiley and Sons. https://doi.org/10.1002/9781118202470.ch3.

3

DIELECTRIC SPECTROSCOPY OF GLASSY DYNAMICS

P. LUNKENHEIMER, M. KÖHLER, S. KASTNER, AND A. LOIDL

3.1 INTRODUCTION

When a liquid becomes a glass, its viscosity shows a tremendous *continuous* variation from values around 10^{-4} Pas for the low-viscosity liquid to $\sim 10^{12}$ Pas at the glass transition temperature and even exceeding values of 10^{15} Pas deep in the solid glass state. This mirrors the so far only poorly understood continuous slowing down of molecular dynamics, which is characteristic of the glass transition [1–3]. One of the best suited methods to follow this change in dynamics in a range as broad as possible is dielectric spectroscopy [4, 5]. If the slowing down entities forming the glass (atoms, ions, molecules, polymer chains, etc.) are charged or exhibit a dipolar moment and are coupled to the structural relaxation, this technique allows direct access to the molecular dynamics, which is characterized by the so-called α-relaxation time τ_α. In dielectric spectroscopy, the response of the sample to an AC electrical field is detected by measuring quantities like the complex dielectric constant or the conductivity. Modern developments in experimental techniques nowadays enable measurements at AC field frequencies varying over more than 18 decades [4, 6], which implies that the molecular dynamics can be followed over a comparable dynamic range.

Already in the mid of the last century, when dielectric spectroscopy started to become a common technique for the investigation of glass-forming materials, there was increasing evidence that their molecular dynamics is more complex than expected and that there is more in glassy dynamics than only the simple translational molecular motion that determines the viscosity [7, 8]. It soon became obvious that between the

Structural Glasses and Supercooled Liquids: Theory, Experiment, and Applications, First Edition.
Edited by Peter G. Wolynes and Vassiliy Lubchenko.

glass transition temperature T_g and the virtual melting point the molecular dynamics exists at all timescales between 100 s and picoseconds. Nowadays it is clear that many different dynamic processes with different timescales exist in glassy matter, mostly faster than expected from the translational molecular motion (termed α-relaxation) alone [1–4, 6]. For about two decades, the investigation of these fast processes belongs to the most active fields of glass physics. They are believed to be the key to a better understanding of the still widely mysterious glass transition phenomenon and are extensively treated in a large variety of different theoretical and phenomenological approaches. In the present work, we will discuss the basics of dielectric spectroscopy of glassy matter, including the measurement and interpretation of the α-relaxation, and we will especially focus on the fast glassy dynamics, providing current experimental results and a comparison with the predictions within modern theoretical concepts.

3.2 DIELECTRIC SPECTROSCOPY

Dielectric spectroscopy is one of the most widely applied techniques for the investigation of glassy dynamics (for an overview, see Refs. 4, 5). The broad accessible frequency range, which is unsurpassed by any other experimental method, makes it ideally suited to follow the slowing down of the α-relaxation dynamics during the transition from the low-viscosity liquid to the solid glass state [4–6]. Dielectric spectroscopy is mostly performed in frequency domain, that is, the measurements are carried out in dependence of the frequency of the applied AC field. For glassy matter, the most commonly measured quantity is the complex dielectric permittivity $\varepsilon^* = \varepsilon' - i\varepsilon''$. To characterize the dynamics of a glass former, usually the imaginary part ε'', termed dielectric loss, is plotted versus the logarithm of frequency ν. It is a measure of the field energy dissipated in the sample (of course, there is no "loss" of energy, but the dissipation leads to a heating of the sample). According to the fluctuation–dissipation theorem [9], any dynamic "process," that is, any time-dependent fluctuation of particles within the sample, will lead to an enhancement of the loss when the field frequency matches the frequency of this fluctuation. In this way, for example, the α-relaxation leads to a peak in plots of ε'' versus log ν. From its peak frequency ν_α, the relaxation time can be estimated via $\tau_\alpha = 1/(2\pi\nu_\alpha)$.

For a thorough investigation of glassy dynamics by dielectric spectroscopy, it is essential to cover a frequency range as broad as possible. To achieve this goal, a combination of techniques is necessary, allowing the so-called "broadband" spectroscopy. Most broadband dielectric spectra reported in literature extend to frequencies up to some gigahertz and have low-frequency limits in the millihertz to hertz range. Pointing out the broadband character of these spectra is justified as standard devices for dielectric measurements cover ranges of hertz–megahertz and measurements at lower and especially those at higher frequencies are relatively demanding. Investigations at even higher frequencies, bridging the gap to the far-infrared region (starting at approximately terahertz), which is covered by commercial infrared spectrometers, are performed only by very few groups worldwide.

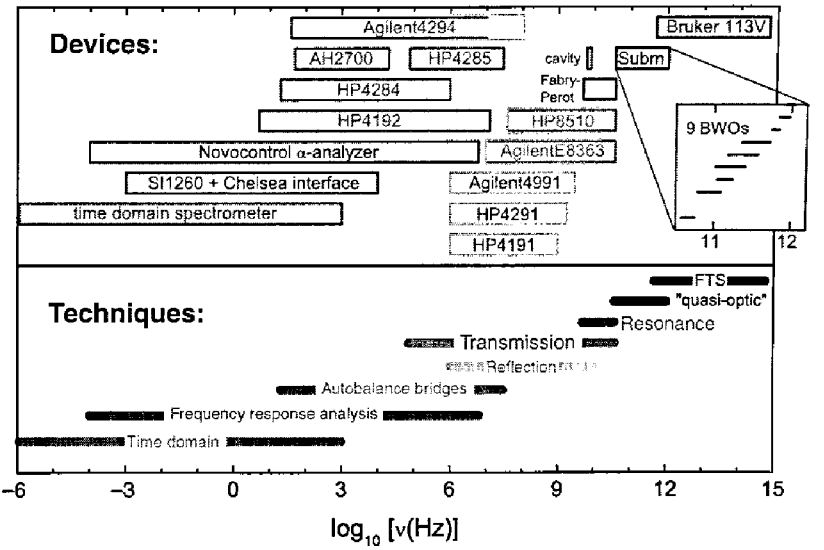

FIGURE 3.1 Overview of the devices and techniques used in the dielectric laboratory at the University of Augsburg for broadband dielectric spectroscopy. At low frequencies a homemade time domain spectrometer and two frequency–response analyzers (Novocontrol Alpha Analyzer and Schlumberger-Solartron SI1260 with Chelsea Dielectric Interface) are used [10]. In addition, various autobalance bridges from Agilent (4294A), Andeen-Hagerling (AH2700A), and Hewlett-Packard (4192A, 4284A, and 4285A) are employed [10]. Several impedance analyzers (4991A, 4291A, and 4191A) and network analyzers (8510C and E8363B) from Agilent and Hewlett-Packard are available for coaxial reflection measurements [10, 11]. The network analyzers are also used for coaxial transmission measurements, a cavity perturbation technique, and a Fabry–Perot resonator setup (Damaskos Model 900T Open Resonator) in the gigahertz range [10, 14, 15, 16]. Toward higher frequencies, a quasi-optical submillimeter wave spectrometer is utilized [17]. The inset in the upper panel shows the frequency ranges of the different radiation sources (backward wave oscillators (BWOs)). The highest frequencies are covered by a modified Bruker IFS 113v Fourier transform infrared spectrometer (FTS). See color version of the figure in Color Plate section.

In Figure 3.1, the experimental techniques and devices used in the Augsburg dielectric group covering frequencies from about 10^{-6} to 10^{15} Hz are shown [4, 10]. Depending on frequency range, different sample geometries are necessary, as schematically indicated in Figure 3.2. At low frequencies, up to several megahertz, a parallel plate capacitor geometry is used (Fig. 3.2a). For samples that are liquid at room temperature, a variety of specially designed parallel plate capacitors are available, which are filled with the sample material. For the detection of low dielectric losses, which, for example, can arise at low temperatures, small plate distances and large areas of the capacitor plates are necessary. Using, for example, glass fibers as spacers, capacitances of the empty capacitor up to some hundred picofarad can be reached. Solid samples are prepared as platelets and covered at opposite sides with

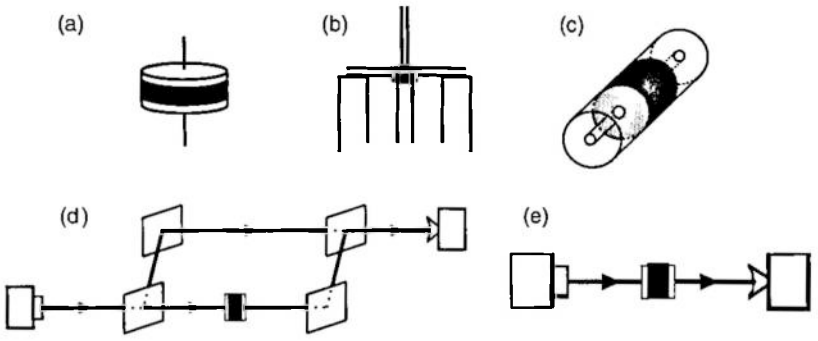

FIGURE 3.2 Schematic drawing of the typical sample geometries used for the different measurement techniques (the sample material is indicated by the filled black regions). (a) Parallel plate capacitor for frequency–response analysis and autobalance bridges [10]. (b) Setup for coaxial reflection measurements where the sample forms the end of the inner conductor (other configurations can also be used) [10, 11]. (c) Coaxial transmission line filled with sample material [10, 16]. (d) Scheme of the Mach–Zehnder spectrometer used for measurements in the submillimeter wavelength range [17]. (e) Setup as used for transmission measurements in the Fourier transform infrared spectrometer (FTS).

an electrode material serving as capacitor plates. These capacitor-shaped samples can be investigated by three techniques: For lowest frequencies, a time domain technique is employed, where the time-dependent charging or discharging of the capacitor is monitored. A Fourier transform leads to the frequency-dependent quantities. This method allows a rather quick collection of data even at very low frequencies, but is of limited precision only. Alternatively, the capacitance C' and conductance G' of the sample capacitor can be measured in dependence of frequency. From these quantities, ε' and ε'' are easily calculated via $\varepsilon' = C'/C_0$ (C_0 the empty capacitance) and $\varepsilon'' = G'/(2\pi\nu C_0)$. The measurements can be performed by frequency–response analysis, which is essentially a lock-in-based technique using commercially available analyzers and provides a very high experimental resolution. Alternatively, various LCR meters using autobalance bridge techniques are available covering a range of hertz–megahertz and allowing a rather quick collection of spectra with a precision sufficient for most applications.

In the less-often covered frequency region of about 1 MHz to some 10 GHz, coaxial reflection techniques are most commonly employed. In this technique, the material under investigation is mounted at the end of a coaxial line bridging inner and outer conductors (Fig. 3.2b). The line is connected to the test port of an impedance or a network analyzer and the electromagnetic wave traveling along the line is reflected by the sample. Either the complex reflection coefficient of this setup is measured or direct current–voltage measurement techniques are used to detect quantities as capacitance and conductance, from which the dielectric permittivity or other material properties can be calculated. The coaxial line is needed to achieve a thermal decoupling of the sample, which is mounted in a cooling or heating device and the test port of the measuring device. A suitable construction of this coaxial line is prerequisite for

the successful application of this technique [11]. Another important aspect of this method is the proper mounting of the sample, for example, as small parallel plate capacitor with a self-constructed termination of the coaxial line or as small droplet that is directly applied to the inner conductor (Fig. 3.2b) [10, 11]. In a variant of this technique, sometimes termed "open-end" coaxial technique, the end of the coaxial line is simply immersed into the liquid sample material or pressed on a flat surface of a solid sample [12, 13]. In all cases, a careful calibration of these coaxial setups is necessary, to correct for any contributions of the coaxial line itself and of the sample holders. Under ideal conditions and if the coaxial line and sample holders are well constructed, these coaxial methods can be used up to some 10 GHz, at least if the loss of the sample is not too small.

Better suited to cover frequencies in the microwave range up to about 50 GHz are resonance and transmission techniques. For resonance measurements, the sample is put into the region of maximum field in a resonator and the resonance frequency and quality factor and determined, for example, by a network analyzer, from which all electrical material parameters can be determined [14]. Resonators usually operate at a single frequency only, which makes the covering of a broad frequency range a tedious task. However, multiple resonances of varying order at different frequencies can also be used, for example, in Fabry–Perot resonators [15]. In transmission measurements, the sample material is filled into a coaxial line or waveguide (Fig. 3.2c) [4, 10, 16]. This is relatively straightforward for liquid samples, but needs easy machinability for solid samples. The transmission of the lines is measured by a network analyzer after proper calibration. Using formulas taking into account multiple reflections within the line, the dielectric material properties can be determined.

The rarely investigated gap between these microwave techniques and the start of the frequency range covered by commercial infrared spectrometers can be closed by using free wave techniques. Here the transmission of unguided electromagnetic waves through the sample or their reflection from the sample is detected. For this purpose, spectrometer setups known from optics can be applied, for example, the Mach–Zehnder geometry as used by the Augsburg dielectric group, where both transmission and phase shift are measured (Fig. 3.2d) [17]. These techniques are sometimes called "quasi-optical" or "THz spectroscopy." The spectrometers are adapted to the much longer wavelengths of this radiation compared to optical experiments (millimeter and submillimeter waves) by using, for example, lenses being made from Teflon and beam splitters being formed by fine wire grids. Unwanted diffraction effects are a critical issue here and the samples have to be of sufficient size to allow proper measurements. Convenient radiation sources used for such types of spectrometers are, for example, backward wave radiators (BWOs), which have a rather large output power in the range of up to 10 mW. With a frequency range tunable by about a factor of 2, several measurements with different BWOs are necessary to cover the complete spectral range of this spectrometer of 40 GHz–1.5 THz (see inset of Fig. 3.1). For the measurements, liquid samples have to be filled into cuvettes. Then the results have to be corrected for the contributions of the windows (including multiple reflections), whose properties can be determined by measurements of the empty cuvettes. More details on this rather sophisticated technique can be found in Refs. 10, 17.

Finally, at the highest frequencies from the far infrared to the optical range, a large variety of commercial devices are available. In our case, a Fourier transform spectrometer is employed (Fig. 3.2e) [4, 10]. One problem with this technique is the necessity to use a Kramers–Kronig transformation to calculate the phase shift because only the absolute value of the transmission is directly measured. Some care has to be taken concerning a proper choice of low- and high-frequency extrapolations of the transmission, which is necessary for the Kramers–Kronig transformation and can have considerable influence on the calculated dielectric parameters.

The investigation of the glass transition with spectroscopic methods not only needs to cover a broad frequency range but also the temperature has to be varied. Glass formers can be found with glass temperatures from cryogenic temperature up to some hundred degrees of Celsius and thus in our group a variety of different heating and cooling devices are used. This includes liquid He cryostats (1.4 –310K), closed-cycle refrigerators (10–310K), nitrogen gas cryostats (100–650K), and various ovens (300–1500K).

As mentioned above, the presence of dipolar or charged entities is prerequisite to enable the investigation of glassy dynamics with dielectric spectroscopy. However, when employing this technique for the investigation of glassy dynamics, one has to be aware that a decoupling of the dynamics detected by dielectric spectroscopy and the "true" dynamics determining, for example, the viscosity can occur. In dipolar glass formers, dielectric spectroscopy primarily probes the reorientational motions of the molecules that are often, but not always, coupled to the translational motions, which constitute the glass transition. In glass formers with mobile ions, the translational motion of these ions is directly probed by dielectric spectroscopy, but under certain circumstances, the ionic motion itself can decouple from the dynamics leading to the glass transition (e.g., if ions of different sizes are present, the smaller ones may move much faster than the larger ones, whose motions govern the viscosity).

3.3 THE PHENOMENOLOGY OF GLASSY DYNAMICS AS REVEALED BY DIELECTRIC SPECTROSCOPY

Figure 3.3 provides a schematic view of the frequency dependence of the dielectric loss in a glass former composed of dipolar molecules. In (a)–(d), the situations for different temperature regimes are depicted, including the crystallized state (d). This figure reveals all features of glassy dynamics, such as α-relaxation, excess wing, β-relaxation, fast process, and boson peak, which will be treated in detail in the following sections. In Figure 3.3a, the situation at high temperatures, deep in the liquid state, is shown. The α-relaxation peak is located at very high frequencies, which mirrors the high molecular mobility in the low-viscosity liquid. The so-called boson peak, a relatively broad excitation in the infrared regime whose origin is still controversially discussed, is partly hidden under the α-peak. Except for intramolecular modes, which have no connection to the glass transition, no further processes show up. Figure 3.3b [4, 6] shows the situation in a supercooled liquid that has been cooled to a relatively low temperature, close to the glass temperature, where

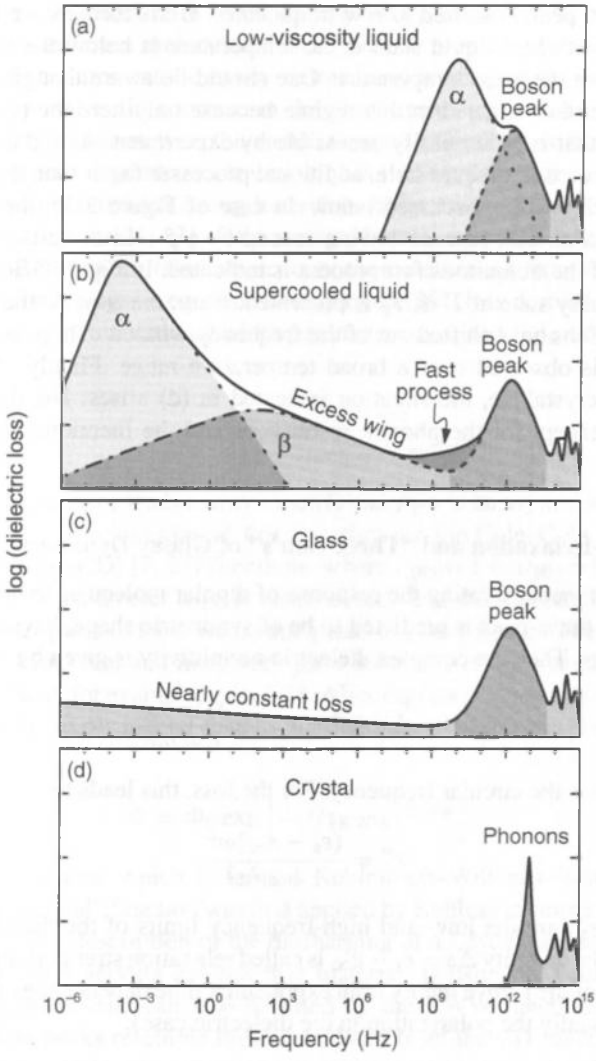

FIGURE 3.3 Schematic illustration of the frequency-dependent dielectric loss in glass-forming materials as observed in broadband dielectric measurements. In frames (a)–(d), the situations for different states of the material are shown. (a) The low-viscosity liquid at high temperatures. (b) The supercooled liquid regime between T_g and the temperature of fusion [4, 6]. (c) The glass significantly below T_g. (d) The crystallized state. The contributions from various dynamic processes are indicated by different shades of gray: The α-relaxation, the β-relaxation, the fast process, the boson peak, and the infrared bands caused by intramolecular resonances. In (b) a situation is shown where the β-relaxation is partly submerged under the dominating α-relaxation process and therefore shows up as a so-called excess wing. Here a single secondary relaxation is assumed; however, additional ones can arise. See color version of the figure in Color Plate section.

the α-relaxation peak is shifted to low frequencies. Glass formers are considered to be in their supercooled liquid state if the temperature is below the temperature of fusion but above the glass temperature. One should be aware that glassy dynamics has mostly been investigated in this regime because only here the relaxation times are in a range that is rather easily accessible by experiment. As indicated in Figure 3.3b, in the supercooled liquid state, additional processes faster than the α-relaxation show up, which will be discussed below. In case of Figure 3.3b, the typical spectrum of a material with an excess wing caused by a β-relaxation is shown and the contribution of the ubiquitous fast process is indicated. In Figure 3.3c, the situation deep in the glassy state at $T \ll T_g$ is presented. Here, the α-peak and possible secondary relaxations have shifted out of the frequency window. Then, usually a nearly constant loss is observed over a broad temperature range. Finally, if the material is allowed to crystallize, the situation indicated in (d) arises: No significant excitations exist, except for the phonon resonances and the mentioned intramolecular modes.

3.3.1 The α-Relaxation and "Three Non's" of Glassy Dynamics

In the simplest theory treating the response of dipolar molecules to an AC field, the Debye theory, the α-peak is predicted to be of symmetric shape, having a half width of 1.14 decades. Then the complex dielectric permittivity is given by

$$\varepsilon^* = \varepsilon' - i\varepsilon'' = \varepsilon_\infty + \frac{\varepsilon_s - \varepsilon_\infty}{1 + i\omega\tau}. \tag{3.1}$$

Here, $\omega = 2\pi\nu$ is the circular frequency. For the loss, this leads to

$$\varepsilon'' = \frac{(\varepsilon_s - \varepsilon_\infty)\omega\tau}{1 + \omega^2\tau^2}. \tag{3.2}$$

Here, ε_s and ε_∞ are the low- and high-frequency limits of the dielectric constant, respectively (the quantity $\Delta\varepsilon = \varepsilon_s - \varepsilon_\infty$ is called relaxation strength). In time domain, the prediction of the Debye theory is an exponential time dependence of the measured quantity Φ (usually the polarization in the dielectric case):

$$\Phi = \Phi_0 e^{-t/\tau}. \tag{3.3}$$

It can be simply derived by assuming that the return rate to equilibrium, after a molecule has been excited (e.g., by the application of a voltage to a capacitor filled with the material), is proportional to its distance from this equilibrium state. However, Equations 3.2 and 3.3 are only rarely fulfilled and in most experiments peaks that are much broader and even asymmetric are instead observed. This behavior is usually termed nonexponentiality and considered as a hallmark feature of glassy matter [1–3]. It is one of the "three non's" [18] referred to in the heading of this section.

For many decades, only speculations concerning the microscopic reason for this deviation of the α-relaxation from Debye theory were possible. One possible explanation is a distribution of relaxation times, that is, each single molecule relaxes with

exponential time dependence as in the Debye theory, however, the relaxation times are different for different molecules (heterogeneous scenario) [19, 20]. This variation of relaxation times can be easily rationalized bearing in mind the disordered nature of glassy matter. In contrast, in the "homogeneous scenario," it is assumed that each molecule relaxes with the same relaxation time, but with an intrinsically nonexponential time dependence. It was only in the last decade that various sophisticated experiments provided strong hints that the heterogeneous scenario is in fact the correct description [21–23] (for a recent alternative approach, combining both scenarios, see Ref. 24). To take into account these deviations from the Debye case, often the Havriliak–Negami equation is employed [25]. It is derived from Equation 3.1 by introducing two additional width parameters α_{HN} and β_{HN}, both smaller than unity:

$$\varepsilon^* = \varepsilon_\infty + \frac{\varepsilon_s - \varepsilon_\infty}{[1 + (i\omega\tau_{HN})^{1-\alpha_{HN}}]^{\beta_{HN}}}. \tag{3.4}$$

Here, the parameter α_{HN} leads to a symmetric and β_{HN} to an asymmetric broadening of the loss peaks. Special cases of this equation are the Cole–Cole (CC) [26] and the Cole–Davidson (CD) [7, 27] functions, where $\beta_{HN} = 1$ or $\alpha_{HN} = 0$, respectively. In most cases, the parameter α_{HN} is close to zero and the CD function provides a satisfactory description of the α-relaxation peaks in glassy matter. The deconvolution of Equation 3.4 into real and imaginary parts leads to a rather complex expression, which can be found, for example, in Ref. 28. Also, Equation 3.3 can be easily modified to account for the experimental data by introducing an additional parameter $\beta_{KWW} < 1$ [29, 30]:

$$\Phi = \Phi_0 \exp\left[-(t/\tau_{KWW})^{\beta_{KWW}}\right]. \tag{3.5}$$

This time dependence, which is termed Kohlrausch–Williams–Watts (KWW) or "stretched exponential" function was first applied by Kohlrausch more than 150 years ago [29, 31] for the description of the discharging of a Leyden jar, an early form of capacitor with glass serving as dielectric material. If using its Fourier transform, frequency-dependent data can also be fitted by the KWW function. Qualitatively, the obtained loss peaks resemble those calculated from the CD function: There is a linear increase at the low-frequency flank of the peak and a power law $\nu^{-\beta}$ at the high-frequency flank. However, both peak shapes are not completely identical. Some efforts have been made to calculate the parameters of the CD or the KWW function from the parameters of the other function [32, 33]. The KWW function is one example for a nonexponential relaxation as considered in the homogeneous scenario mentioned above. However, it should be noted that neither the use of Equation 3.5 nor the use of Equation 3.4 implies any preference for the homogeneous or heterogeneous scenario, because both are primarily phenomenological functions. Especially, Equation 3.5 can also be seen as resulting from a distribution of relaxation times, which is more in line with the current understanding of the deviations from the Debye case [20].

One should be aware that the relaxation times obtained from fits of loss peaks with different functions (e.g., CC, CD, and KWW) can significantly differ from each

other. Assuming a disorder-induced distribution of τ, as discussed above, for most formulas employed to describe relaxation peaks, an average relaxation time $\langle\tau\rangle$ can be calculated [32, 34]. For example, from the width parameter β_{CD} and relaxation time τ_{CD} of the CD function, $\langle\tau\rangle = \beta_{CD}\tau_{CD}$ can be obtained. For all functions, the average relaxation rate $1/(2\pi\langle\tau\rangle)$ is usually a good approximation of the peak frequency. Thus, $\langle\tau\rangle$ is best suited to compare relaxation times obtained from different fit procedures or by simply reading off the peak frequencies.

The temperature dependences of the characteristic times of the different dynamic processes in glass formers are often summarized in so-called relaxation maps, where the logarithm of the relaxation times is plotted versus the inverse temperature (Arrhenius representation). Figure 3.4 schematically shows the typical temperature development of the most common processes in glassy matter. The naive expectation for $\tau_\alpha(T)$ in this representation is a straight line behavior, which would correspond to

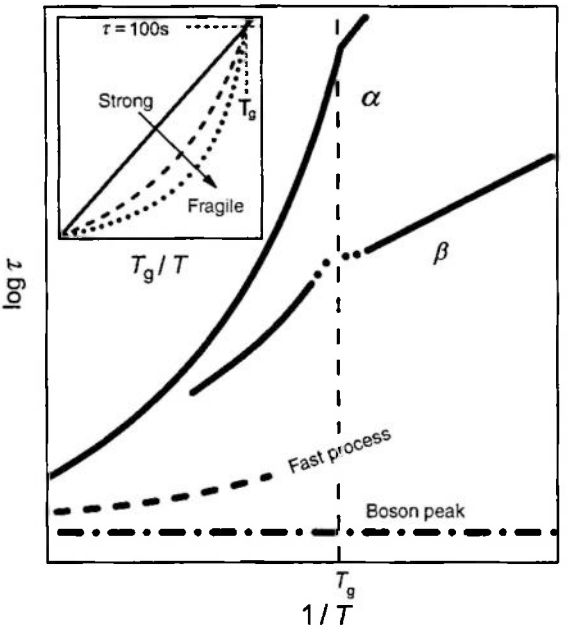

FIGURE 3.4 Schematic relaxation map (relaxation times versus inverse temperature) of commonly observed relaxation phenomena in glass-forming materials. At temperatures above the glass transition temperature T_g, the α- and β-relaxation times often show a stronger temperature dependence than expected for a simple thermally activated behavior. In the glass state, the β-relaxation time is known to show Arrhenius behavior and the α-relaxation also seems to behave that way. Close to T_g, the temperature dependence of the β-relaxation is unclear (sometimes a minimum is observed) [85, 90]. The boson peak is nearly temperature independent. To tentatively assign a relaxation time to the fast process, the minimum frequency was taken. The inset shows an Angell plot [45] of the α-process where the temperature axis is scaled with T_g. The typical behavior of strong and fragile glass formers is indicated.

an Arrhenius law, $\tau \sim \exp[E/(k_B T)]$. Here, E is an energy barrier hindering the motion of the relaxing entities (reorientation of molecules in the dielectric case). However, the α-relaxation time in most cases shows significant deviations from a straight line behavior in this representation, as indicated in Figure 3.4. In addition to the nonexponentiality treated above, this non-Arrhenius behavior (the second "non" [18]) is another hallmark feature of glassy dynamics [1]. An often advanced phenomenological viewpoint to explain this type of temperature dependence may be summarized as follows: The increase of the slope of the $\log[\tau_\alpha(1/T)]$ curve for decreasing temperature may be regarded as indicative of an increase of the effective energy barrier hindering the relaxation. This may signify the fact that at lower temperatures, the different molecules are far from relaxing independent of each other, but their motions become increasingly cooperative. Quite generally, cooperativity is considered as an important aspect to explain the glass transition.

There are numerous theoretical approaches of glassy dynamics aiming to explain the temperature dependence of τ_α [18, 35]. The highest α-relaxation times detected by dielectric spectroscopy are about 10^6 s [36] and the lowest ones reach down to about 10^{-11} [4, 37, 38]. The theoretical description of a quantity that varies over 17 decades is a highly demanding task and in fact most theoretically derived expressions work only well in part of the range that is covered in the best investigated materials. An astonishingly successful parameterization of $\tau_\alpha(T)$ data is provided by the phenomenological Vogel–Fulcher–Tammann (VFT) law [39]:

$$\tau = \tau_0 \exp\left[\frac{DT_{VF}}{T - T_{VF}}\right]. \tag{3.6}$$

Here, T_{VF} and D are termed Vogel–Fulcher temperature and strength parameter, respectively. Despite its simplicity, the VFT equation works relatively well, but here deviations may also show up, at least if considering data from broadband measurements extending over many decades of τ_α. Often, at high temperatures, a crossover into Arrhenius behavior may be suspected or even two different VFT laws are employed to take into account the experimental curves [40]. The transition temperatures between these different regimes are sometimes considered to be of importance for understanding the glass transition [41–43]. The VFT law seems to imply a divergence of the relaxation time at $T = T_{VF}$ (which, however, cannot be experimentally checked because the glass falls out of equilibrium long before reaching T_{VF}). This may be interpreted as indication of a phase transition at $T_{VF} < T_g$, which, however, is avoided for dynamical reasons. Thus, the VFT law gives support to theories as, for example, the Adam–Gibbs theory or the free volume theory [35] that assume such a transition underlying the evolution of the glass state. In this context, it is of interest that in a recent work [44], reviewing dielectric α-relaxation time data of numerous glass formers, it was concluded that there is in fact no real compelling experimental evidence for the divergence of τ_α suggested by the VFT law.

Different glass formers show different degrees of deviation of their temperature-dependent α-relaxation times from the Arrhenius law. This can best be visualized by comparing different $\tau(T)$ curves in a scaled representation, termed Angell plot

[45], as schematically shown in the inset of Figure 3.4. Here, the logarithm of τ is plotted versus T_g/T, which corrects for the wide range of glass temperatures found for different materials. Glass formers, whose relaxation time curves do not or only weakly deviate from linear behavior in the Angell plot, are termed "strong" and those that exhibit a strong curvature are termed "fragile." Many properties, even if their relation to the α-relaxation time is not immediately obvious, correlate with the classification of a glass as strong or fragile. Examples are the specific heat anomaly at the glass transition [46], the width parameter of the α-relaxation [47], or the strength of the boson peak [48]. The deviation from the Arrhenius behavior can be quantified by the strength parameter of Equation 3.6 [49] or by determining the slope at T_g of the curves in the Angell plot, leading to the fragility index m [50].

Finally, we would like to mention a third "non," characteristic of glassy dynamics, the nonergodicity. All glasses are far from thermodynamic equilibrium and if the temperature in a glass forming system falls below the glass temperature, ergodicity becomes broken [1, 2, 51]. This is practically unavoidable because when approaching the glass temperature, the relaxation time becomes exceedingly large (cf. Fig. 3.4). Thus, when further cooled below T_g, the material cannot accommodate for the continuously falling temperature anymore. For example, its molecules become so immobile that they are hindered to fully perform the structural rearrangements that give rise to the thermal contraction of the volume, which therefore shows a weaker temperature dependence at $T < T_g$. Weaker temperature dependences of physical quantities are quite a general phenomenon when a supercooled liquid transfers into a glass. As indicated in Figure 3.4, the α-relaxation time also shows such behavior [52–54]. As glasses are not in equilibrium, their physical properties vary with time. At temperatures not too far below T_g, this time dependence, termed aging, can be experimentally observed. Dielectric spectroscopy can also be used to investigate the aging of glasses [36, 55–57]. From the analysis of the time dependence of the loss, a relaxation time can be determined, which is found to be in good agreement with the α-relaxation times determined in equilibrium above the glass transition [36].

3.3.2 The β-Relaxation and the Excess Wing

As noted above, a variety of additional processes are observed at frequencies beyond the α-peak, which all lead to additional contributions in the loss. Many of this faster dynamics that is typical for glass-forming matter were first found by dielectric spectroscopy. Among the most important ones are the secondary relaxation processes that are thought to be inherent to the glassy state of matter (termed slow β-relaxations or Johari–Goldstein (JG) processes [58]) and the so-called excess wing. The β-process shows up as additional peak or shoulder in $\varepsilon''(\nu)$, typically located in the kilohertz–megahertz region, at higher frequencies than the α-peak [56, 58–61]. Its amplitude is usually significantly weaker than that of the α-peak. In the example schematically shown in Figure 3.3b, instead of a β-relaxation peak or shoulder, a second power law at the high-frequency flank of the α-peak shows up [4, 62, 63]. For this feature, our group has termed the expression "excess wing" [64] as it appears as excess intensity

at the high-frequency wing of the α-peak. It was shown by Nagel and coworkers that α-peak and excess wing show intriguing scaling properties [65].

As for the β-relaxation, the origin of the excess wing is highly debated. Both features have in common that they are rather universal and it seems that each glass-forming material has at least either an excess wing or a β-relaxation (both cases are sometimes referred to as "type A" and "type B," respectively [59]). Thus, it seems natural to assume that both spectral features are of same origin and that the excess wing simply arises from a β-relaxation peak that is partly submerged under the α-peak, as indicated in Figure 3.3b. Indeed, there is now ample evidence, initiated by aging measurements [66] and corroborated by various other experiments [61, 67–69], that the excess wing can be ascribed to a secondary relaxation process. However, it is an open question if this process is indeed a JG β-relaxation [66, 70] or a further separate phenomenon [59, 71].

It should be noted that secondary relaxations have different origins. One of them being intramolecular modes, for example, side chain motions of polymers. From the viewpoint of glass science, such types of secondary relaxations, which also often are termed β-relaxation, are of less interest. However, in a seminal work [58], Johari and Goldstein demonstrated that β-relaxations also show up in materials, where such internal modes are unlikely to occur. To distinguish this type of relaxation, inherent to the glassy state of matter, from the mentioned internal modes, they are sometimes termed JG β-relaxations. There is no consensus concerning their microscopic origin. One possible explanation is in terms of "island of mobility;" that is, in the glass-forming materials, local regions are assumed where the molecules have higher mobility and these molecules give rise to the β-relaxation [58]. In contrast, another explanation assumes that *all* molecules contribute to the β-relaxation via motions on a smaller length scale than the α-relaxation [72–74]. There the multiwell energy landscape experienced by the molecules is assumed to have a fine structure with smaller local energy minima. Then, the β-relaxation arises from transitions between these local minima. For the reorientational processes probed by dielectric spectroscopy, these transitions correspond to small-angle rotations. Various other approaches for the explanation of the excess wing and the β-relaxation were also proposed, for example, within the dynamically correlated domain model [75]. Recently, some efforts have also been made to explain the JG process and excess wing within the framework of the mode coupling theory (MCT) [76], which may be regarded as a highly sophisticated theory of the glass transition and glassy dynamics. Recent extensions of the coupling model also offer an explanation of the JG relaxation [70, 77–79], assuming independent (i.e., noncooperative) processes to cause this feature [79].

One should note that both the JG β-relaxation and an intramolecular (or other) relaxation mode can simultaneously arise in a material [43, 80, 81]. Moreover, it was suggested that the excess wing is caused by a separate relaxation that can occur in addition to the JG relaxation [59]. Thus, there may be some confusion concerning the naming of these relaxations and in literature there is no consistent use of nomenclature. In our view, the most reasonable solution is to label secondary relaxations with β, γ, and so on in accordance with the order of their appearance in the spectrum.

In addition to the microscopic origin of the JG β-relaxation, its behavior in the so-called merging region is also highly debated [82–85]. The β-relaxation time τ_β has a weaker temperature dependence than the α-relaxation (cf. Fig. 3.4). This leads to a successive convergence of the α- and JG β-relaxation times with increasing temperature. Finally, at high temperatures, deep in the liquid state, merging occurs, that is, both relaxation peaks cannot be distinguished anymore [57, 58, 82, 85, 86]. At low temperatures, $\tau_\beta(T)$ usually follows simple thermally activated behavior (signified by the linear behavior in Fig. 3.4) [57, 58, 59, 85, 87, 88] and this finding often is taken as characteristic property of this type of relaxation. However, one should note that it is mainly based on data obtained below the glass temperature where both relaxations are well separated. Close to and above T_g, the evaluation of $\tau_\beta(T)$ becomes difficult due to the overlap with the α-peak. Above the glass temperature, $\tau_\beta(T)$ seems to change into a stronger temperature dependence than Arrhenius [6, 57, 69, 70, 85, 87–89]. This can be explained within the framework of the coupling model [70, 77, 79]. In the region around T_g, the behavior is unclear. There is some evidence [57, 85, 90–92] that a minimum in $\tau_\beta(T)$ may occur close to T_g. This scenario was rationalized within the so-called minimal model [90]. Alternatively, an "encroachment" of the relaxation time of a γ-relaxation with the JG relaxation was proposed [92].

3.3.3 The Fast Process

Mode coupling theory [93–95], the most prominent theory of the glass transition, predicts additional spectral contributions due to a fast process, also termed fast β-relaxation, at very high frequencies of about 100 MHz–1 THz. It is thought to arise from a "rattling" movement of a particle in the transient "cage" formed by its neighbors. It was mainly this theoretical prediction that has triggered the enormous interest in the behavior of glassy matter in this rarely investigated fast dynamical regime. Indeed, evidence for the fast process was soon found, mainly by scattering methods [96–98] as dielectric spectroscopy at such high frequencies is a rather demanding task. Nevertheless, technical advances have also allowed performing nearly continuous dielectric measurements in this range, and nowadays the detection of fast glassy dynamics with this technique has also become a well-established fact [4, 37, 38, 91, 99, 100]. It is now generally accepted that spectra in the 100 MHz–1 THz region (whatever technique may be used for their determination) can only be explained by assuming some excess intensity due to one or more fast processes.

Without assuming any fast dynamics, in this region a loss minimum is expected. Depending on material and temperature, its low-frequency wing should be caused by one of the processes treated above, that is, the α-relaxation peak, the JG β-peak, any other type of secondary relaxation, or the excess wing. Its high-frequency wing should correspond to the increase toward the so-called boson peak, which is known to occur at some terahertz (see below). In Figure 3.3b, this situation is indicated by the dashed line around 10^{10} Hz. A minimum indeed is experimentally observed; however, it is clearly too shallow to be explained in such a trivial way [4, 37, 38, 91, 99, 100]. This finding evidences an additional contribution, caused by a fast process, as schematically indicated in Figure 3.3b. As demonstrated for several glass formers,

its spectral form and temperature dependence are in accord with the predictions of the MCT [2, 37, 91, 99–102].

In addition to MCT, there are also other approaches to explain the experimental findings. Especially, within the extended coupling model [79], a nearly constant loss contribution is assumed to explain the shallowness of the minimum. This is schematically shown in Figure 3.5a (no JG process or excess wing is included here, that is,

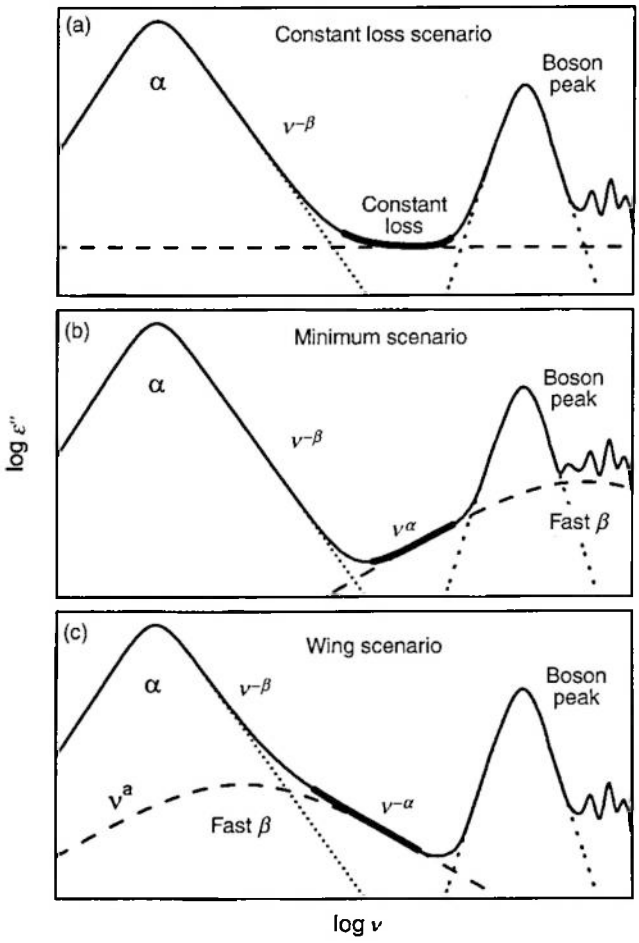

FIGURE 3.5 Schematic loss spectra of different scenarios explaining the excess intensity in the gigahertz–terahertz region (fast process). In (a), a constant loss contribution is assumed [79, 103, 104, 106, 107]. Parts (b) and (c) [122] show two scenarios of MCT assuming that the fast process gives rise to a CC peak [76]. Depending on the frequency of the CC peak, the conventional case of a minimum [94] (b) or a wing at the high-frequency flank of the α-peak [76] (c) can arise. The excess contribution obtained for these three scenarios is indicated by the bold lines.

the situation at high temperatures is shown, where these features have merged with the α-relaxation). The occurrence of a constant loss is a long-standing concept in glass physics and was already considered, for example, in Refs. 103, 104. Within the coupling model, it is ascribed to "caged dynamics," quite similar to the fast β-process within MCT [79]. Using such a constant loss contribution, the high-frequency minimum region of broadband dielectric spectra has successfully been described for several glass formers [99, 105–107].

MCT in its most simplified form predicts that the fast process manifests itself in the minimum region, which can be approximated by the sum of two power laws. MCT makes distinct predictions concerning the two exponents and the temperature development of minimum frequency and amplitude. However, in two recent works [76], it was shown that the fast β-process in fact can lead to a peak whose spectral form is well approximated by a CC function (Equation 3.4 with $\beta_{HN} = 1$). Two scenarios can arise: The peak is located at extremely high frequencies and only its left wing is visible. This is schematically shown in Figure 3.5b (a high-temperature situation is assumed here, where a possible excess wing or the β-relaxation is merged with the α-relaxation). It corresponds to the conventional sum of two power laws situation mentioned above and shown in Figure 3.3b, which is routinely applied to fit such data. However, a completely different situation was also considered, namely, that the CC peak is located at much lower frequency [76]. In this case, only its high-frequency wing may be visible, as shown in Figure 3.5c, or if not shifted to quite as low frequencies, it could lead to a shoulder or secondary peak. While there is no clear experimental proof for the occurrence of the latter case so far [52, 108], it is interesting that in this way the MCT may explain the excess wings or the JG β-relaxations showing up in most glass formers. However, a situation like in Figure 3.3b, where both an excess wing and the excess intensity in the minimum region simultaneously occur cannot be accounted for within this scenario.

3.3.4 Beyond the Minimum

As mentioned above, at frequencies beyond the minimum in the terahertz frequency region, another clearly developed peak arises (Fig. 3.3), usually termed boson peak. It is another example of a characteristic feature of glassy dynamics that can be considered as unexplained as no consensus concerning its microscopic origin has been achieved so far. Its name arises from the fact that it was first found by Raman experiments at low frequencies, where it revealed a temperature dependence in accord with Bose–Einstein statistics [109]. (Some information on the detection of the boson peak with dielectric spectroscopy and on the justification of referring to the observed loss peak as boson peak can be found in Ref. 110.) The excitations causing the boson peak also lead to the commonly found excess contribution of glassy matter to specific heat measurements at low temperatures [111]. Among the models considered for its explanation are the soft potential model [112, 113], phonon localization models [114, 115], a harmonic oscillator model with a distribution of force constants [116], and the MCT [117]. As it is seldom investigated by dielectric spectroscopy, it will be only briefly treated in the present work. Finally, at infrared and optical frequencies,

intramolecular excitations show up (see Fig. 3.3 at $\upsilon > 30$ THz), which remain nearly unaffected by the glass transition and thus here are not of further interest.

3.4 BROADBAND DIELECTRIC SPECTRA OF GLASS-FORMING LIQUIDS

In the following, we will provide several examples of experimental data from dielectric spectroscopy showing the various dynamic processes treated in the preceding section. Figure 3.6a and b provides broadband loss spectra of two typical glass-forming liquids, namely, propylene glycol (PG) ($C_3H_8O_2$, $T_g \approx 167$K) [91] and xylitol ($C_5H_{12}O_5$, $T_g \approx 248$K) [57], measured at various temperatures. The chosen materials are representative examples for small-molecule organic glass formers with a relatively high dipolar moment and good glass-forming ability as regularly investigated by dielectric spectroscopy. The present spectra cover a significantly extended frequency range compared to previous investigations of these materials [59, 61, 70, 84, 91, 118, 119]. While in PG an excess wing is observed at the high-frequency flank of the α-peak

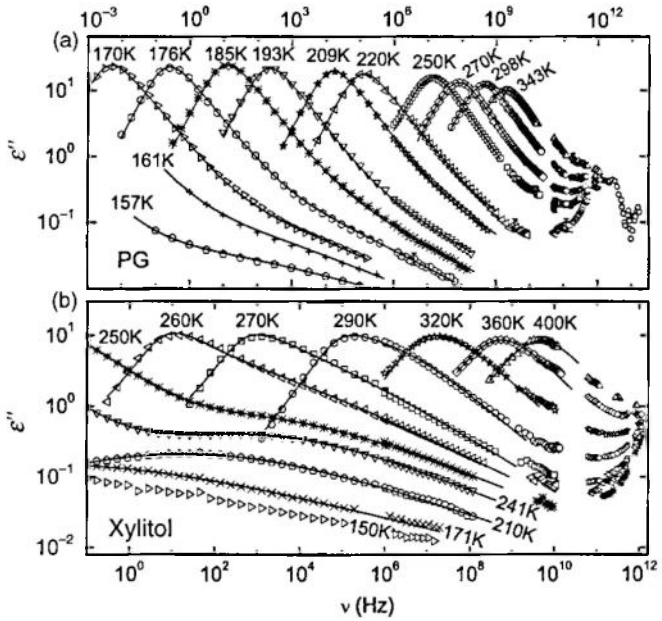

FIGURE 3.6 Broadband dielectric loss spectra of propylene glycol (a) and xylitol (b) for various temperatures. The solid lines are fits with the sum of a CD and CC function for α- and β-relaxations, respectively. In (b), above 300K, a HN function had to be used instead of a CD function. The frequency-dependent spectra of propylene glycol are partly published in Ref. 91 and those of xylitol see in Ref. 57.

(type A), xylitol shows additional peaks at low and shoulders at high temperatures revealing the presence of a well-pronounced β-relaxation (type B).

3.4.1 The α-Relaxation

In both examples shown in Figure 3.6, the dominating feature of the spectra is the α-relaxation peak. For a linear scaling of the ordinate, as regularly found in older dielectric publications [7, 26, 120], all additional features beyond these peaks are hardly visible. Depending on measurement temperature, the α-peaks arise at frequencies located well in the gigahertz range at high temperatures, but at low temperatures, they are even shifted out of the covered low-frequency limit of about 10 mHz. This tremendous but continuous variation of the peak frequencies, triggered by temperature changes on the order of a factor of 2 only, is the signature of the glass transition occurring in these materials. It directly mirrors the glassy freezing of the molecular dynamics that occurs at this continuous transition from the low-viscosity liquid to the solid glass. Irrespective of the additional spectral features following at higher frequencies (excess wing or β-relaxation), the α-peaks are asymmetric and broader than expected for the Debye case. Their low- and high-frequency flanks are linear in the double-logarithmic representation of Figure 3.6 and thus can be described by power laws with positive or negative exponents, respectively. The low-frequency exponent is found to be close to 1 while the absolute values of the high-frequency ones, however, are smaller than 1. Such a behavior is often found in glass-forming liquids and is just the behavior following from the CD formula (Eq. 3.4) with $\alpha_{HN} = 0$) or the Fourier transform of the KWW function (Eq. 3.5). Indeed, using the sum of a CD function and additional contributions to account for the high-frequency processes (see below), the α-peaks revealed in Figure 3.6 can be well fitted (solid lines).

The most significant parameter obtained from the fits of the loss spectra is the relaxation time. In Figure 3.7, the average α-relaxation times obtained for PG and xylitol are shown in an Arrhenius representation (open triangles and circles, respectively) [36, 57, 91]. In both cases, a pronounced non-Arrhenius behavior is found. In addition to the analysis of dielectric spectra, relaxation times can also be determined from aging measurements [36]. Figure 3.8 shows time-dependent measurements of ε'' during recovery of equilibrium after quickly cooling the samples to a temperature below T_g [36, 57]. The lines are fits with a modified KWW law taking into account the fact that the relaxation time itself varies under aging, as discussed in detail in Ref. 36. The fits provide an equilibrium relaxation time, which can be assumed to be identical to the α-relaxation times as determined from frequency-dependent equilibrium measurements because both mirror structural rearrangement processes. However, equilibrium measurements at temperatures below T_g are impracticable because of the long waiting time necessary to reach equilibrium and the long measuring times needed to detect the α-peak, which at $T < T_g$ is located at very low frequencies. Thus, aging measurements as shown in Figure 3.8 are the most feasible way to extend $\tau_\alpha(T)$ curves to longer relaxation times than usually covered by dielectric spectroscopy. The relaxation times indicated by the closed symbols in Figure 3.7 were obtained from the aging data of Figure 3.8. Indeed, they provide a reasonable extension of the $\tau(T)$ curves

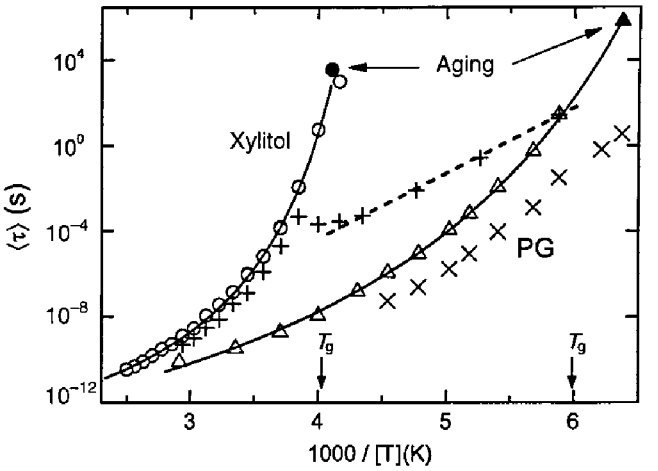

FIGURE 3.7 Temperature-dependent relaxation times τ_α (open symbols) and τ_β of xylitol (plus symbols) and propylene glycol (crosses) in Arrhenius representation [36, 57, 91]. The closed symbols for the α-relaxation were obtained from long-time aging experiments [36]. The solid lines are fits with a VFT law for the α-relaxation [57, 91]. The dashed line demonstrates Arrhenius behavior of $\tau_\beta(T)$ in xylitol at low temperatures. From the slope, an energy barrier of 0.61 eV was determined.

from equilibrium measurements. Only the relaxation time value, determined from the frequency-dependent measurements of xylitol at 241K ($1000/T = 4.15\text{K}^{-1}$), does not match the general trend of the data points obtained at higher temperatures and the single point from aging. To understand this deviation, it should be noted that 241K is below $T_g = 248$K and, thus, the sample was not in thermodynamic equilibrium during this measurement. As indicated in Figure 3.4, $\tau_\alpha(T)$ tends to a weaker temperature

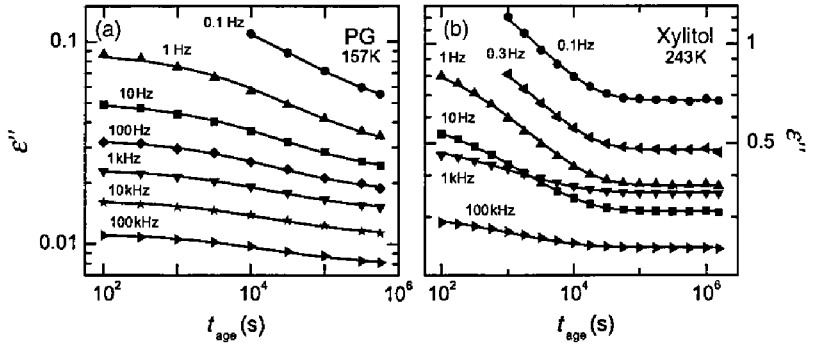

FIGURE 3.8 Time-dependent loss of glassy propylene glycol [36] and xylitol [57] for various frequencies, measured during aging below T_g. The lines are fits with a modified KWW law [36, 56, 57].

dependence in out-of-equilibrium measurements, which explains the observed deviation. Only from aging measurements, reliable information on the relaxation time significantly below T_g can be obtained [121].

As demonstrated by the solid lines in Figure 3.7, the complete experimental data, extending over 13 decades for xylitol and 15 decades for PG can be relatively well fitted by the VFT equation (Eq. 3.6). There are other examples of glass formers where the VFT equation provides less perfect fits of the experimental data. Also, in the present case, small deviations of fits and experimental data occur that, however, do not become obvious in the scale of Figure 3.7. For a detailed discussion of deviations from VFT behavior, see, for example, Ref. 40. In Figure 3.9, the relaxation time data of PG and xylitol are shown in an Angell plot. This figure also includes data on several other dipolar small-molecule glass formers measured in the Augsburg dielectric laboratory [36, 89, 91, 122]. Various degrees of deviation from Arrhenius behavior can be easily discerned. The fragilities m, determined from the slope at $T_g/T = 1$, range from $m = 48$ for PG up to $m = 133$ for sorbitol.

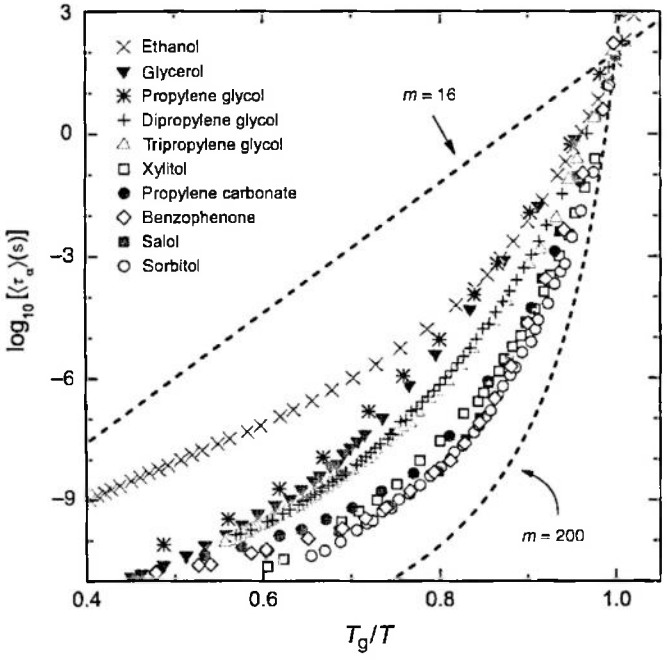

FIGURE 3.9 Angell plot of the α-relaxation times of various structural glass formers investigated in the Augsburg dielectric group [4, 36, 57, 91, 108, 140]. The dashed lines demonstrate the behavior for minimal and very large fragility. The glass transition temperatures used to scale the data are 99K (ethanol), 186K (glycerol), 167K (propylene glycol), 194K (dipropylene glycol), 189K (tripropylene glycol), 248K (xylitol), 156K (propylene carbonate), 207K (benzophenone), 218K (salol), and 268K (sorbitol).

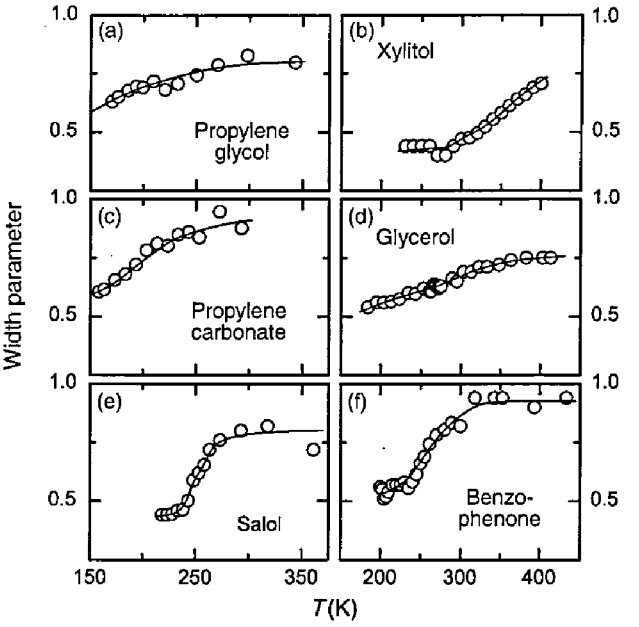

FIGURE 3.10 Width parameters of the α-process for six glass formers as obtained from fits of the dielectric loss spectra (the data for propylene glycol [91], propylene carbonate [4], glycerol [4], and benzophenone [108] have previously been published). The width parameter is given by β_{CD} for fits with the CD function and by $\beta_{HN}(1 - \alpha_{HN})$ for fits with the HN function. The lines are drawn to guide the eyes.

Another parameter obtained from fits of the α-relaxation peaks is the width parameter β_{CD} or β_{KWW} of Equations 3.4 and 3.5, respectively (as mentioned above, α_{HN} is close to zero in most cases). Figure 3.10 shows some examples of $\beta_{CD}(T)$ for various dipolar glass formers, including PG and xylitol. In cases where the HN function was employed to fit the spectra, instead of β_{CD} the quantity $\beta_{HN}(1 - \alpha_{HN})$ is provided. Just as $-\beta_{CD}$ in case of the CD function, $-\beta_{HN}(1 - \alpha_{HN})$ is the exponent of the high-frequency power law of the α-peak. As long as α_{HN} is small, this quantity is best suited to compare width parameters from fits with the CD and HN functions. As demonstrated in Figure 3.10, in most glass formers, the width parameter is found to increase with increasing temperature. Its deviation from unity, that is, the nonexponentiality of glassy dynamics, can be explained by a distribution of relaxation times caused by disorder (heterogeneous scenario; see Section 3.3.1). Having this in mind, the increase of the width parameter may be attributed to the fact that when approaching the low-viscosity liquid regime, the very fast molecular fluctuations may blur any heterogeneity in the materials and each relaxing entity essentially senses the same environment. However, within this picture, the Debye case, that is, $\beta_{CD} = 1$, should be approached, while in fact a constant high-temperature value somewhat below unity is experimentally observed in many glass formers (Fig. 3.10). It should also be

mentioned that there are various approaches, both phenomenological and theoretical, that assume that the so-called time–temperature superposition principle should be obeyed, which implies that the width parameter of the α-peaks is constant, at least in certain temperature ranges [74, 94, 123]. The marked temperature dependence of the width parameters found in many publications seems to speak against such a scenario, but it may be ascribed to the influence of additional processes having an impact on the high-frequency flank of the α-peaks. A clarification of this question is not within the scope of the present work. Here we only want to remark that in using as few parameters as possible to describe the experimental data without invoking additional processes, an increase of the width parameter with temperature followed by a saturation at values below unity seems to be a rather universal feature of glassy matter. In a recent work, this behavior was rationalized within a model assuming intrinsic nonexponentiality and a distribution of Vogel–Fulcher temperatures [24].

In Figure 3.11, the temperature-dependent relaxation strengths of the same materials as in Figure 3.10 are shown. In general, when collecting $\Delta\varepsilon(T)$ data on different glass formers, no universal characteristics typical for glassy matter are revealed. Instead details of molecular interactions and correlation effects in the specific materials often seem to dominate the relaxation strength. Neglecting such interactions, within the time-honored Onsager theory, a Curie law $\Delta\varepsilon \propto 1/T$ is expected [28]. Indeed, in many glass formers, $\Delta\varepsilon$ is found to increase with decreasing temperature (Fig. 3.11). However, often a stronger temperature dependence that sometimes can be parameterized by a Curie–Weiss type of behavior $\Delta\varepsilon \propto 1/(T - T_{CW})$ and may indicate cooperative relaxation processes is found (solid lines in Fig. 3.11). MCT makes distinct predictions for the temperature dependence of the relaxation strength. For discussions of some of the data sets of Figure 3.11 within this framework, see Refs. 37, 108, 124.

3.4.2 The Excess Wing and the β-Relaxation

As mentioned above, PG and xylitol are nice examples for the appearance of an excess wing or a β-relaxation in broadband spectra of glass-forming liquids (Fig. 3.6). The excess wing in PG (Fig. 3.6a) shows up as a shallow power law (i.e., a linear decrease in the double-logarithmic representation of Fig. 3.6a) in excess to the high-frequency flank of the α-relaxation peaks. It is best seen at low temperatures and the absolute value of its exponent, that is, its slope in Figure 3.6a, increases when the temperature rises. Finally, at about 220–250K, it becomes indistinguishable from the high-frequency flank of the α-peak. As discussed in Section 3.3.2, the excess wing can be ascribed to a secondary relaxation peak that is partly submerged under the dominating α-peak. The α- and β-relaxation times are usually close to each other at high temperatures, but become successively separated at low temperatures (cf. Fig. 3.4). Thus, it is natural to perform measurements at as low as possible temperatures to disclose the β-peak despite the dominating α-peak. However, at temperatures below the glass transition, the material falls out of equilibrium and measurements after long aging times are necessary to take advantage of this intrinsic separation of both peaks. In Figure 3.12a spectra in the excess wing region of PG at $T < T_g$ are shown [70, 125]. The uppermost curve was measured directly after cooling down to 157K. It shows

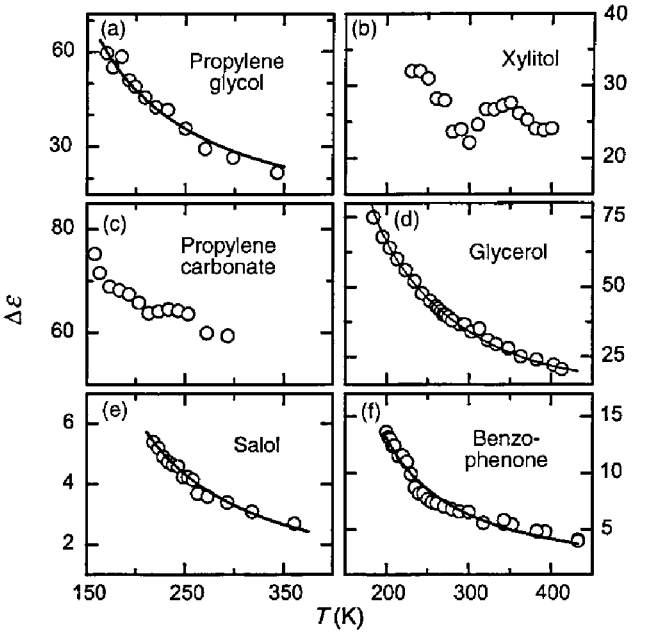

FIGURE 3.11 Relaxation strengths of the α-process of six different glass formers as obtained from fits of the dielectric loss spectra (the data for propylene glycol [91], propylene carbonate [107], glycerol [6], and benzophenone [108] have been previously published). The solid lines in (a) [91], (d) [107], (e), and (f) [108] are fits using the Curie–Weiss law. The corresponding Curie–Weiss temperatures are 53K (propylene glycol), 97K (glycerol), 90K (salol), and 107K (benzophenone).

the power law, typical for the excess wing. The sample was kept at this temperature for 7 days and further spectra were collected at regular time intervals. As revealed in Figure 3.12a, significant aging effects show up and the power law observed at the shortest times develops into a significant shoulder when equilibrium is approached at the longest times. This shoulder is a clear hint to a secondary relaxation causing the excess wing. Similar results were also obtained for various other glass formers [66, 125]. It was noted in Section 3.3.2 that it is not self-evident that this excess wing relaxation is of JG type, that is, a β-relaxation inherent to the glass transition, which is found in many type B systems. To identify "true" JG relaxations, a criterion was proposed in Ref. 77, which is based on an empirically found correlation of the JG relaxation time with β_{KWW} at the glass temperature [78] and which can be rationalized within the framework of the coupling model [79]. Based on these considerations, in Ref. 70 it was shown that the secondary relaxation causing the excess wing in PG most likely is of JG type.

From spectra of type B glass formers, where β- and α-relaxations are well separated, it is known that the CC function usually provides good fits of the β-peaks [57, 59, 61, 87, 88]. Thus, the data on PG at temperatures up to 220K were fitted with the

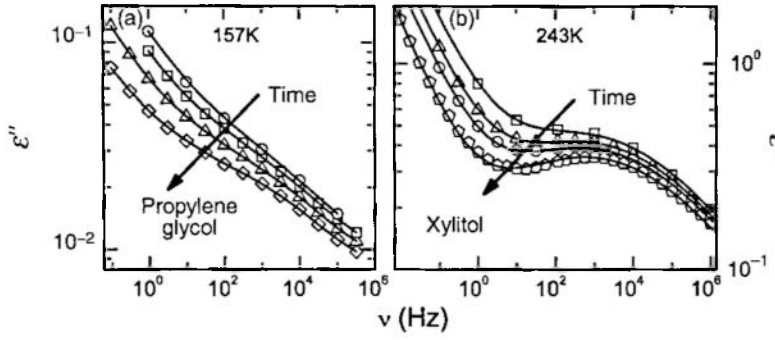

FIGURE 3.12 Spectra of the dielectric loss in the excess wing region of propylene glycol (a) [70, 125] and in the β-peak region of xylitol (b) [57] measured during aging at $T < T_g$ at various aging times. The lines are fits using the sum of a CC function and a power law taking into account the α-peak, which is shifted beyond the lower frequency limit of the measurement. The aging times of the shown curves are (from top to bottom) $\log_{10}[t_{age}(s)] = 2.5, 3.5, 4.5, 5.75$ for propylene glycol and $\log_{10}[t_{age}(s)] = 2, 3, 3.5, 6.2$ for xylitol.

sum of a CD function (for the α-peaks) and a CC function (for the β-peak causing the excess wing) [70, 91, 126]. At higher temperatures, where the excess wing has merged with the α-peak, a single CD function was used. As demonstrated by the solid lines in Figure 3.6a, good fits of the experimental data extending up to the minimum region could be achieved in this way. The resulting relaxation times of the JG β-relaxation in PG are included in Figure 3.7 (crosses). For all temperatures, they are relatively close to the α-relaxation times. This reflects the observed overlap of the α- and β-relaxation peaks in this material, leading to the observation of an excess wing instead of a β-peak. Above T_g, $\tau_\beta(T)$ exhibits significant deviations from Arrhenius behavior as also found in other glass formers [6, 57, 70, 84, 89, 108]. As mentioned in Section 3.3.2, these findings can be rationalized within the coupling model, which predicts a correlation of the β-relaxation time with τ_α and the width parameter of the α-relaxation peaks [70, 77–79].

In contrast to PG, the broadband spectra of xylitol (Fig. 3.6b) reveal a well-pronounced secondary relaxation (type B glass former [61, 85, 127]), which was identified as being of JG type [77, 85, 127]. It is most pronounced at low temperatures and shows the usual merging with the α-peak at high temperatures. One should note, however, that the data at $T < 250$K were measured below the glass temperature ($T_g = 248$K) and thus do not reflect the equilibrium properties of xylitol. In Figure 3.12b, different spectra in the β-peak region, measured during aging at 243K, are provided [57]. As in PG (Fig. 3.12a), in this type B glass former, the α- and β-peaks also separate during aging: While the curves at short times only exhibit a shoulder due to the overlap with the α-peak, the equilibrium curve obtained after 18 days clearly shows a peak. Thus, the occurrence of a β-peak is a true equilibrium feature of xylitol. Another interesting aspect of these results is the finding that the β-peak frequency does not or only very weakly shift during aging. So far it is not clear if this is a general

property of β-relaxations and contradictory results on the aging of β-relaxations have been reported in literature [58, 77, 128–131].

The solid lines in Figure 3.6b are fits with the sum of a CD (or HN at $T > 300$K) and a CC function at $T < 340$K and a single HN function at $T > 340$K, providing a reasonable description of the spectra up to the minimum region. The resulting β-relaxation times are shown in Figure 3.7 (plus symbols). The linear behavior observed at low temperatures, deep in the glass regime, signifies thermally activated dynamics as often found for β-relaxations below T_g [59, 85, 87, 88]. From the slope of the dashed line in Figure 3.7, an energy barrier of 0.61 eV is obtained. Around the glass temperature, a minimum shows up in $\tau_\beta(T)$ as was previously observed in other glass formers [85, 90–92] and explained by different models [90, 92]. At $T > T_g$, the β-relaxation times closely approach the $\tau_\alpha(T)$ curve. However, one has to be aware that in this region there is a high uncertainty in the determination of τ_β due to the strong overlap with the α-relaxation. Comparing the behavior of PG and xylitol in Figure 3.7, it becomes obvious that in the latter, close to and below T_g, a much larger separation of the α- and β-timescales arises. In the type-B glass-former xylitol, this leads to the clear evolution of a β-peak in the spectra of Figure 3.6b; while in the type A system PG (Fig. 3.6a), an excess wing is all that remains visible of the β-relaxation.

3.4.3 The Fast Process and the Boson Peak

In Figure 3.13, the minimum region of the loss spectra of PG and xylitol (Fig. 3.6) is shown in more detail. With increasing temperature, the minimum shifts to higher frequencies and its amplitude increases. Similar behavior is quite universally found in other glass formers also, both by dielectric [4, 37, 38, 91, 99, 100] and other spectroscopic methods [96–98, 101, 102, 132, 133]. In PG, the measurements at room temperature were extended well into the infrared range revealing a second peak at about 3 THz. It evidences the boson peak as detected in various glass formers, not only by scattering techniques [96–98, 132, 133] but also by dielectric spectroscopy [4, 37, 110]. Using scattering techniques, the boson peak is usually detected in the scattering function S, plotted versus frequency. The susceptibility χ'' ($=\varepsilon''$ for dielectric spectroscopy) and S are approximately related via $\chi'' \propto \nu S$ [133]. Thus, as was pointed out in Ref. 133, for $S(\nu)$ to exhibit a peak, at its left wing χ'' must increase stronger than linear. This is indeed what is frequently observed experimentally [4, 97, 98, 133]. Therefore, the most shallow loss minimum that could arise without invoking any additional fast processes should be composed from a linear increase accounting for the low-frequency flank of the boson peak and a power-law decrease ν^{-b} accounting for any low-frequency contributions. Depending on the material (type A or B) and the temperature (below or above merging temperature), the latter could be the excess wing, the high-frequency flank of the β-peak or that of the α-peak. Thus, we arrive at

$$\varepsilon'' = c_b \nu^{-b} + c_n \nu, \tag{3.7}$$

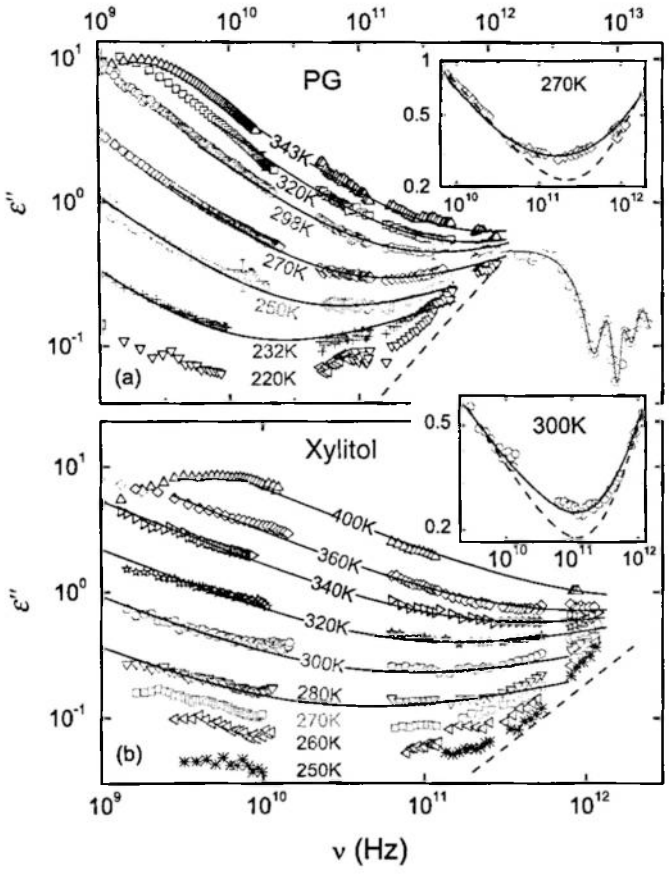

FIGURE 3.13 Dielectric loss spectra of propylene glycol (a) [91] and xylitol (b) [57] at high frequencies, in the minimum and boson peak region. The solid lines are fits of the minimum region with the MCT prediction, Equation 3.9, using identical parameters a and b for all temperatures. The dashed lines illustrate a linear increase of $\varepsilon''(\nu)$. The solid line in the infrared region is a guide to the eye. The insets demonstrate that the simple superposition ansatz, Equation 3.7, is not sufficient to explain the shallow minimum (dashed lines). The solid lines in the inset are fits using Equation 3.8, including an additional constant loss contribution.

where c_b and c_n are prefactors. As shown in the insets of Figure 3.13 for a typical loss minimum, for both materials this approach (dashed lines) is not in accord with the experimentally observed spectra. A similar behavior was found in all glass formers investigated in the minimum region by our group so far [4, 37, 91, 100, 105, 107]. This finding clearly proves that an additional process must be active at these high frequencies. There are only few definite model predictions for this region. One of them is provided by the extended coupling model, which uses a constant loss contribution, attributed to "caged dynamics," to account for the observed shallowness of the minima [79]. This corresponds to the scenario schematically shown in Figure 3.5a. Indeed, in

most cases by introducing a constant loss parameter ε_c, the formula

$$\varepsilon'' = c_b \nu^{-b} + c_n \nu, + \varepsilon_c \tag{3.8}$$

is able to provide a satisfactory description of the experimental data [4, 99, 105–107]. As an example for the suitability of this approach, corresponding fits (solid lines) are shown in the insets of Figure 3.13.

The first theory to predict excess intensity in the minimum region of the susceptibility was the MCT. As noted in Section 3.3.3, the most basic version of the MCT (sometimes termed idealized MCT) makes detailed predictions on the spectral shape and temperature evolution of the loss minimum [93, 94, 134]. Especially, a sum of two power laws

$$\varepsilon'' = \frac{\varepsilon_{\min}}{a+b}\left[a\left(\frac{\nu}{\nu_{\min}}\right)^{-b} + b\left(\frac{\nu}{\nu_{\min}}\right)^{a}\right], \tag{3.9}$$

with both exponents a and b correlated with each other and identical for all temperatures is expected. This corresponds to the scenario shown in Figure 3.5b. In addition, a critical temperature development is predicted for the frequency position $\nu_{\min}$ and amplitude $\varepsilon_{\min}$ of the minimum and also for the α-peak position $\nu_\alpha \approx 1/(2\pi\langle\tau_\alpha\rangle)$. Fits of the temperature dependences of these quantities should reveal a critical temperature $T_c > T_g$, which can be regarded as a kind of idealized glass transition temperature. Finally, it is another rather restricting prediction of the MCT that the critical exponents determined from the temperature dependences of the minimum and α-peak frequencies should be directly related to the power-law exponents of the minimum (Eq. 3.9). For a more detailed account of these MCT predictions and a comparison with dielectric high-frequency data, the reader is referred, for example, to Refs. 4, 105.

For the present cases of PG and xylitol, fits with the power-law sum of MCT are shown as solid lines in Figure 3.13. The fits were performed simultaneously for all temperatures, with the exponents related to each other by the MCT prediction (i.e., only one of the two exponents is a free parameter). It should be noted that Equation 3.9 is an approximation and expected to be valid at $T > T_c$ and in vicinity of the minimum only. Thus, the spectra at lower temperatures were not fitted and deviations of the fit curves at low and high frequencies were admitted. As revealed by Figure 3.13, the fits with Equation 3.9 work well over about 2–3 decades of frequency, which is as good as or better than in most other glass formers investigated so far [4, 37, 91, 99, 100, 105]. The resulting temperature-dependent minimum frequencies and amplitudes are shown in Figure 3.14, together with the α-peak frequencies ν_α. Here representations were chosen that should lead to linear behavior for the critical laws predicted by MCT and a crossing of the abscissa at $T = T_c$ [93, 94, 134]. The solid lines shown in Figure 3.14 demonstrate that the data can be consistently described with the same T_c for all quantities [57]. We arrive at $T_c = 239$K for PG [91] and $T_c = 308$K for xylitol. For PG, some inconsistent T_c values were reported earlier, ranging from 198 to 314K [120, 135–137]. For xylitol, to our knowledge, there are no literature data on T_c. The

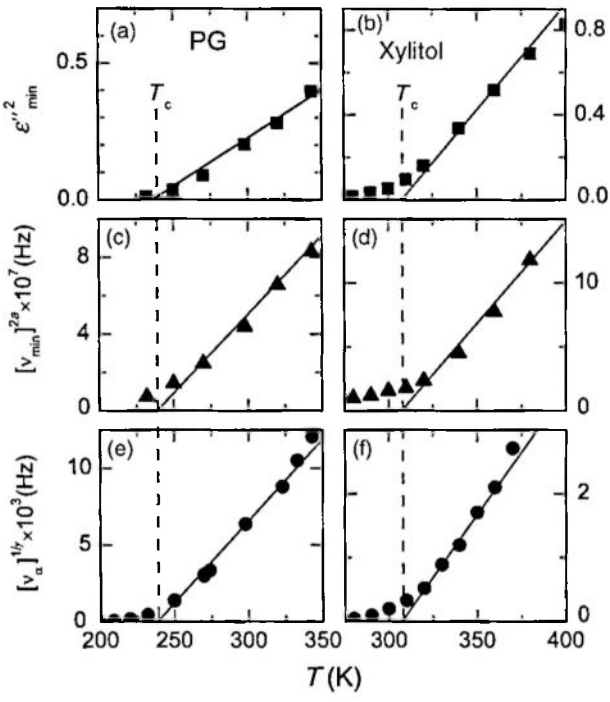

FIGURE 3.14 Temperature dependence of the amplitude ε_{min} (a and b) and position ν_{min} (c and d) of the $\varepsilon''(\nu)$ minimum and of the α-relaxation rate ν_α (e and f) of propylene glycol [91] and xylitol [57]. ε_{min} and ν_{min} have been taken from the fits with Equation 3.9, as shown in Figure 3.13. Representations have been chosen that should result in linear behavior according to the predictions of the MCT. The solid lines demonstrate a consistent description of all three quantities with a T_c of 239K for propylene glycol and 308K for xylitol.

critical behavior in Figure 3.14 breaks down at low temperatures and, especially for ν_α, at high temperatures also, deviations show up. However, it should be noted that the critical MCT laws should hold for temperatures above but close to T_c only. Overall, the critical laws of MCT in these two materials are as well fulfilled as for most other glass formers reported in literature. An evaluation within idealized MCT, as presented here, is a standard procedure for a quick check of the consistency of experimental data with MCT and for obtaining a first estimate of the critical temperature. Nevertheless, it has to be clearly stated that only an analysis within advanced MCT concepts can reveal definite information and a simultaneous evaluation of results obtained with different experimental methods can also be very helpful, which, however, is out of the scope of the present work. For examples of such more sophisticated treatments, the reader is referred to Refs. 101, 102, 138.

In the two presented glass formers, so far only for PG at room temperature, an infrared measurement revealing the boson peak was performed. To our knowledge, after glycerol [38] and propylene carbonate [37], PG is only the third structural glass

former where broadband dielectric loss data including the boson peak have been provided. Due to the proximity of the α-peak, only a shoulder is in fact seen in the loss spectrum of Figure 3.13a. However, taking into account the only weak temperature dependence of the spectral shape of the boson peak in most glass formers [96, 97, 98, 105, 110, 132, 133], the increase of $\varepsilon''(\nu)$ in the region of 0.1–1 THz measured at the lowest temperatures (Fig. 3.13) can be taken as a good estimate of the low-frequency wing of the boson peak. While in PG, this increase is nearly linear (cf. dashed line), it is somewhat steeper than linear for xylitol ($\varepsilon'' \propto \nu^{1.3}$). In other materials too, variations in the low-frequency wing of the boson peak were found [4, 105, 110]. As mentioned in Section 3.3.4, the boson peak is mainly investigated by scattering methods and its microscopic origin is highly debated. For some discussions of the boson peak detected with dielectric spectroscopy and a possible mechanism for its generation, see Ref. 110.

Beyond the boson peak, a succession of sharp resonance-like features are found (Fig. 3.13a). They arise from internal modes of the PG molecules and are of no further relevance from a glassy dynamics point of view.

3.5 SUMMARY

We have seen that glassy dynamics is complex and comprises a variety of different processes. Broadband spectra measured with dielectric spectroscopy are able to reveal crucial information on all of them. Understanding these processes is commonly considered as prerequisite for achieving a deeper understanding of the glass transition. However, while even for the α-relaxation, there are many open questions, for example, concerning the origin of its non-Arrhenius behavior, the faster processes are far from being understood. It is clear now that the excess wing found in some materials is due to a secondary relaxation. However, it is not clear if this is the same JG β-relaxation as found in numerous other glass formers to give rise to a well-pronounced secondary loss peak. It is clear that the occurrence of the JG β-relaxation is a rather universal feature of glassy dynamics. However, its origin is still controversially debated and even fundamental questions as its generation by part of the molecules only or by all molecules have not yet been clarified. It is clear that fast dynamic processes exist in the gigahertz–terahertz range and also compelling evidence for the boson peak was found in broadband dielectric spectra. However, even for these features of glassy dynamics, still many competing explanations exist.

Irrespective of any microscopic interpretations, it is an interesting fact that the various dynamic processes mentioned above are found in many different classes of glassy matter, such as small-molecule glass formers (e.g., PG and xylitol), polymers, ionic-melt glass formers, metallic glasses [139], or even the so-called plastic crystals where glassy freezing is observed for the orientational degrees of freedom only, while the centers of gravity of the molecules are fixed on their crystal positions [140]. Therefore, glassy dynamics seems to be really universal. This provides strong support for the idea that a general theory can be found for the glass transition and glassy state of matter, independent of any details of the materials investigated [141].

REFERENCES

[1] M. D. Ediger, C. A. Angell, and S. R. Nagel, *J. Phys. Chem.* **100**, 13200 (1996).

[2] C. A. Angell, K. L. Ngai, G. B. McKenna, P. F. McMillan, and S. W. Martin, *J. Appl. Phys.* **88**, 3113 (2000).

[3] K. L. Ngai, *J. Non-Cryst. Solids* **275**, 7 (2000).

[4] P. Lunkenheimer, U. Schneider, R. Brand, and A. Loidl, *Contemp. Phys.* **41**, 15 (2000).

[5] F. Kremer and A. Schönhals (eds), *Broadband Dielectric Spectroscopy*, Springer, Berlin, 2002.

[6] P. Lunkenheimer and A. Loidl, *Chem. Phys.* **284**, 205 (2002).

[7] D. W. Davidson and R. H. Cole, *J. Chem. Phys.* **19**, 1484 (1951).

[8] F. X. Hassion and R. H. Cole, *Nature* **172**, 212 (1953).

[9] S. W. Lovesey, *Theory of Neutron Scattering from Condensed Matter*, Clarendon Press, Oxford, 1984.

[10] U. Schneider, P. Lunkenheimer, A. Pimenov, R. Brand, and A. Loidl, *Ferroelectrics* **249**, 89 (2001).

[11] R. Böhmer, M. Maglione, P. Lunkenheimer, and A. Loidl, *J. Appl. Phys.* **65**, 901 (1989).

[12] Y. Z. Wei and S. Sridhar, *Rev. Sci. Instrum.* **64**, 3041 (1989).

[13] G. Q. Jiang, W. H. Wong, E. Y. Raskovich, W. G. Clark, W. A. Hines, and J. Sanny, *Rev. Sci. Instrum.* **64**, 1614 (1993).

[14] (a) J. C. Slater, *Rev. Mod. Phys.* **18**, 441 (1946). (b) O. Klein, S. Donovan, M. Dressel, and G. Grüner, *Int. J. Infrared Millimeter Waves* **14**, 2423, 2459, 2489 (1993).

[15] (a) L. J. Auchterlonie and I. Y. Ahmed, *J. Phys. E* **10**, 691 (1977). (b) P. K. Yu and A. L. Cullen, *Proc. R. Soc. Lond. A* **380**, 49 (1982). (c) A. C. Lynch, *Proc. R. Soc. Lond. A* **380**, 73 (1982).

[16] A. M. Nicholson and G. F. Ross, *IEEE Trans. Instrum. Meas.* **IM-19**, 377 (1970).

[17] (a) A. A. Volkov, Yu. G. Goncharov, G. V. Kozlov, S. P. Lebedev, and A. M. Prokhorov, *Infrared Phys.* **25**, 369 (1985). (b) A. A. Volkov, G. V. Kozlov, S. P. Lebedev, and A. M. Prokhorov, *Infrared Phys.* **29**, 747 (1989). (c) B. Gorshunov, A. A. Volkov, I. Spektor, A. M. Prokhorov, A. Mukhin, M. Dressel, S. Uchida, and A. Loidl, *Int. J. Infrared Millimeter Waves* **26**, 1217 (2005).

[18] J. C. Dyre, *Rev. Mod. Phys.* **78**, 953 (2006).

[19] R. Richert, *J. Non-Cryst. Solids* **172**, 209 (1994).

[20] For reviews on heterogeneity in glassy matter, see (a) H. Sillescu, *J. Non-Cryst. Solids* **243**, 81 (1999). (b) M. D. Ediger, *Annu. Rev. Phys. Chem.* **51**, 99 (2000).

[21] (a) K. Schmidt-Rohr and H. W. Spiess, *Phys. Rev. Lett.* **66**, 3020 (1991). (b) R. Böhmer, G. Hinze, G. Diezemann, B. Geil, and H. Sillescu, *Europhys. Lett.* **36**, 55 (1996).

[22] B. Schiener, R. Böhmer, A. Loidl, and R. V. Chamberlin, *Science* **274**, 752 (1996).

[23] M. T. Cicerone and M. D. Ediger, *J. Chem. Phys.* **103**, 5684 (1995).

[24] D. Cangialosi, A. Alegria, and J. Colmenero, *J. Chem. Phys.* **130**, 124902 (2009).

[25] S. Havriliak and S. Negami, *J. Polymer Sci. C* **14**, 99 (1966).

[26] K. S. Cole and R. H. Cole, *J. Chem. Phys.* **9**, 341 (1941).

[27] D. W. Davidson and R. H. Cole, *J. Chem. Phys.* **18**, 1417 (1950).

[28] C. J. F. Böttcher and P. Bordewijk, *Theory of Electric Polarization*, Vol. **II**, Elsevier, Amsterdam, 1973.

[29] R. Kohlrausch, *Ann. Phys.* **167**, 56, 179 (1854).

[30] G. Williams and D. C. Watts, *Trans. Faraday Soc.* **66**, 80 (1970).

[31] Instead of Ref. 29, often mistakenly an earlier Kohlrausch work is cited, a fact that is discussed in some detail in *Physik Journal* **3**, 27 (2004).

[32] C. P. Lindsey and G. D. Patterson, *J. Chem. Phys.* **73**, 3348 (1980).

[33] F. Alvarez, A. Alegria, and J. Colmenero, *Phys. Rev. B* **44**, 7306 (1991).

[34] C. T. Moynihan, L. P. Boesch, and N. L. Laberge, *Phys. Chem. Glasses* **14**, 122 (1973).

[35] For a review of various theories of the glass transition, see J. Jäckle, *Rep. Prog. Phys.* **49**, 171 (1986).

[36] P. Lunkenheimer, R. Wehn, U. Schneider, and A. Loidl, *Phys. Rev. Lett.* **95**, 055702 (2005).

[37] U. Schneider, P. Lunkenheimer, R. Brand, and A. Loidl, *Phys. Rev. E* **59**, 6924 (1999).

[38] U. Schneider, P. Lunkenheimer, R. Brand, and A. Loidl, *J. Non-Cryst. Solids* **235–237**, 173 (1998).

[39] (a) H. Vogel, *Phys. Z.* **22**, 645 (1921). (b) G. S. Fulcher, *J. Am. Ceram. Soc.* **8**, 339 (1923). (c) G. Tammann and W. Hesse, *Z. Anorg. Allg. Chem.* **156**, 245 (1926).

[40] (a) F. Stickel, E. W. Fischer, and R. Richert, *J. Chem. Phys.* **102**, 6251 (1995). (b) F. Stickel, E. W. Fischer, and R. Richert, *J. Chem. Phys.* **104**, 2043 (1996).

[41] R. Richert and C. A. Angell, *J. Chem. Phys.* **108**, 9016 (1998).

[42] (a) V. N. Novikov and A. P. Sokolov, *Phys. Rev. E* **67**, 031507 (2003). (b) A. Schönhals, *Europhys. Lett.* **56**, 815 (2001).

[43] S. Capaccioli, M. S. Thayyil, and K. L. Ngai, *J. Phys. Chem. B* **112**, 16035 (2008).

[44] T. Hecksher, A. I. Nielsen, N. B. Olsen, and J. C. Dyre, *Nat. Phys.* **4**, 737 (2008).

[45] (a) W. T. Laughlin and D. R. Uhlmann, *J. Phys. Chem.* **76**, 2317 (1972). (b) C. A. Angell and W. Sichina, *Ann. N.Y. Acad. Sci.* **279**, 53 (1976).

[46] C. A. Angell, *Science* **267** 1924 (1995).

[47] R. Böhmer, K. L. Ngai, C. A. Angell, and D. J. Platzek, *J. Chem. Phys.* **99**, 4201 (1993).

[48] A. P. Sokolov, E. Rössler, A. Kisliuk, and D. Quitmann, *Phys. Rev. Lett.* **71**, 2062 (1993).

[49] C. A. Angell, in K. L. Ngai and G. B. West (eds), *Relaxations in Complex Systems*, National Technical Information Service, Springfield, 1984, p. 3.

[50] (a) D. J. Plazek and K. L. Ngai, *Macromolecules* **24**, 1222 (1991). (b) R. Böhmer and C. A. Angell, *Phys. Rev. B* **45**, 10091 (1992).

[51] L. Cipelletti and L. Ramos, *J. Phys. Condens. Matter* **17**, R253 (2005).

[52] L. C. Pardo, P. Lunkenheimer, and A. Loidl, *Phys. Rev. E* **76**, 030502(R) (2007).

[53] A. Pimenov, P. Lunkenheimer, H. Rall, R. Kohlhaas, A. Loidl, and R. Böhmer, *Phys. Rev. E* **54**, 676 (1996).

[54] A. Pimenov, P. Lunkenheimer, M. Nicklas, R. Böhmer, A. Loidl, and C. A. Angell, *J. Non-Cryst. Solids* **220**, 93 (1997).

[55] R. L. Leheny and S. R. Nagel, *Phys. Rev. B* **57**, 5154 (1998).

[56] P. Lunkenheimer, R. Wehn, and A. Loidl, *J. Non-Cryst. Solids* **352**, 4941 (2006).

[57] (a) R. Wehn, P. Lunkenheimer, and A. Loidl, *J. Non-Cryst. Solids* **353**, 3862 (2007). (b) S. Kastner, M. Köhler, Y. Goncharov, P. Lunkenheimer, and A. Loidl, *J. Non-Cryst. Solids* **357**, 510 (2011).

[58] G. P. Johari and M. Goldstein, *J. Chem. Phys.* **53**, 2372 (1970).

[59] A. Kudlik, S. Benkhof, T. Blochowicz, C. Tschirwitz, and E. Rössler, *J. Mol. Struct.* **479**, 201 (1999).

[60] A. Kudlik, C. Tschirwitz, S. Benkhof, T. Blochowicz, and E. Rössler, *Europhys. Lett.* **40**, 649 (1997).

[61] A. Döβ, M. Paluch, H. Sillescu, and G. Hinze, *Phys. Rev. Lett.* **88**, 095701 (2002).

[62] A. Hofmann, F. Kremer, E. W. Fischer, and A. Schönhals, in R. Richert and A. Blumen (eds), Disorder Effects on Relaxational Processes, Springer, Berlin, 1994, p. 659.

[63] R. L. Leheny and S. R. Nagel, *Europhys. Lett.* **39**, 447 (1997).

[64] R. Brand, P. Lunkenheimer, U. Schneider, and A. Loidl, *Phys. Rev. Lett.* **82**, 1951 (1999).

[65] P. K. Dixon, L. Wu, S. R. Nagel, B. D. Williams, J. P. Carini, *Phys. Rev. Lett.* **65**, 1108 (1990).

[66] U. Schneider, R. Brand, P. Lunkenheimer, and A. Loidl, *Phys. Rev. Lett.* **84**, 5560 (2000).

[67] S. Hensel-Bielowka, S. Pawlus, C. M. Roland, J. Zioło, and M. Paluch, *Phys. Rev. E* **69**, 050501(R) (2004).

[68] J. Mattson, R. Bergman, P. Jacobsson, and L. Börjesson, *Phys. Rev. Lett.* **90**, 075702 (2003).

[69] T. Blochowicz and E. A. Rössler, *Phys. Rev. Lett.* **92**, 225701 (2004).

[70] K. L Ngai, P. Lunkenheimer, C. León, U. Schneider, R. Brand, and A. Loidl, *J. Chem. Phys.* **115**, 1405 (2001).

[71] S. Hensel-Bielowka and M. Paluch, *Phys. Rev. Lett.* **89**, 025704 (2002).

[72] F. H. Stillinger, *Science* **267** 1935 (1995).

[73] (a) M. Vogel and E. Rössler, *J. Chem. Phys.* **114**, 5802 (2001). (b) J. S. Harmon, M. D. Demetriou, W. L. Johnson, and K. Samwer, *Phys. Rev. Lett.* **99**, 135502 (2007).

[74] C. Gainaru, O. Lips, A. Troshagina, R. Kahlau, A. Brodin, F. Fujara, and E. A. Rössler, *J. Chem. Phys.* **128**, 174505 (2008).

[75] (a) R. V. Chamberlin, *Phys. Rev. B* **48**, 15638 (1993). (b) R. V. Chamberlin, *Phys. Rev. Lett.* **82**, 2520 (1999).

[76] (a) W. Götze and M. Sperl, *Phys. Rev. Lett.* **92**, 105701 (2004). (b) M. Sperl, *Phys. Rev. E* **74**, 011503 (2006).

[77] K. L. Ngai and M. Paluch, *J. Chem. Phys.* **120**, 857 (2004).

[78] K. L. Ngai, *Phys. Rev. E* **57**, 7346 (1998).

[79] K. L. Ngai, *J. Phys. Condens. Matter* **15**, S1107 (2003).

[80] M. S. Thayyil, S. Capaccioli, D. Prevosto, and K. L. Ngai, *Philos. Mag.* **88**, 4007 (2008).

[81] M. Paluch, S. Pawlus, S. Hensel-Bielowka, E. Kaminska, D. Prevosto, S. Capaccioli, P. A. Rolla, and K. L. Ngai, *J. Chem. Phys.* **122**, 234506 (2005).

[82] A. Arbe, D. Richter, J. Colmenero, and B. Farago, *Phys. Rev. E* **54**, 3853 (1996).

[83] E. Donth, K. Schröter, and S. Kahle, *Phys. Rev. E* **60**, 1099 (1999).

[84] A. Arbe, J. Colmenero, D. Gómez, D. Richter, and B. Farago, *Phys. Rev. E* **60**, 1103 (1999).

[85] M. Paluch, C. M. Roland, S. Pawlus, J. Zioło, and K. L. Ngai, *Phys. Rev. Lett.* **91**, 115701 (2003).

[86] (a) F. Garwe, A. Schönhals, H. Lockwenz, M. Beiner, K. Schröter, and E. Donth, *Macromolcules* **29**, 247 (1996). (b) F. Alvarez, A. Hofmann, A. Alegria, and J. Colmenero, *J. Chem. Phys.* **105**, 432 (1996).

[87] T. Fujima, H. Frusawa, and K. Ito, *Phys. Rev. E* **66**, 031503 (2002).

[88] R. Nozaki, H. Zenitani, A. Minoguchi, and K. Kitai, *J. Non-Cryst. Solids* **307–310**, 349 (2002).

[89] R. Brand, P. Lunkenheimer, U. Schneider, and A. Loidl, *Phys. Rev. B* **62**, 8878 (2000).

[90] J. C. Dyre and N. B. Olsen, *Phys. Rev. Lett.* **91**, 155703 (2003).

[91] M. Köhler, P. Lunkenheimer, Y. Goncharov, R. Wehn, and A. Loidl, *J. Non-Cryst. Solids* **356**, 529 (2010).

[92] K. L. Ngai, K. Grzybowska, A. Grzybowski, E. Kaminska, K. Kaminski, M. Paluch, and S. Capaccioli, *J. Non-Cryst. Solids* **354**, 5085 (2008).

[93] (a) U. Bengtzelius, W. Götze, and A. Sjölander, *J. Phys. C* **17**, 5915 (1984). (b) E. Leutheusser, *Phys. Rev. A* **29**, 2765 (1984). (c) W. Götze, *Z. Physik B* **60**, 195 (1985).

[94] W. Götze and L. Sjögren, *Rep. Prog. Phys.* **55**, 241 (1992).

[95] W. Götze, *Complex Dynamics of Glass-Forming Liquids*, Oxford University Press, Oxford, 2009.

[96] G. Li, W. M. Du, X. K. Chen, and H. Z. Cummins, *Phys. Rev. A* **45**, 3867 (1992).

[97] (a) G. Li, W. M. Du, A. Sakai, and H. Z. Cummins, *Phys. Rev. A* **46**, 3343 (1992). (b) H. Z. Cummins, W. M. Du, M. Fuchs, W. Götze, S. Hildebrand, A. Latz, G. Li, and N. J. Tao, *Phys. Rev. E* **47**, 4223 (1993).

[98] J. Wuttke, J. Hernandez, G. Li, G. Coddens, H. Z. Cummins, F. Fujara, W. Petry, and H. Sillescu, *Phys. Rev. Lett.* **72**, 3052 (1994).

[99] P. Lunkenheimer, A. Pimenov, M. Dressel, Yu. G. Goncharov, R. Böhmer, and A. Loidl, *Phys. Rev. Lett.* **77**, 318 (1996).

[100] P. Lunkenheimer, A. Pimenov, and A. Loidl, *Phys. Rev. Lett.* **78**, 2995 (1997).

[101] J. Wuttke, M. Ohl, M. Goldammer, S. Roth, U. Schneider, P. Lunkenheimer, R. Kahn, B. Ruffle, R. Lechner, and M. A. Berg, *Phys. Rev. E* **61**, 2730 (2000).

[102] M. Goldammer, C. Losert, J. Wuttke, W. Petry, F. Terki, H. Schober, and P. Lunkenheimer, *Phys. Rev. E* **64**, 021303 (2001).

[103] (a) L. Böhm, D. L. Smith, and C. A. Angell, *J. Mol. Liq.* **36**, 153 (1987). (b) C. Liu and C. A. Angell, *J. Chem. Phys.* **93**, 7378 (1990). (c) C. A. Angell, L. Böhm, M. Oguni, and D. L. Smith, *J. Mol. Liq.* **56**, 275 (1993).

[104] (a) R. H. Cole and E. Tombari, *J. Non-Cryst. Solids* **131–133**, 969 (1991). (b) K. L. Ngai, U. Strom, and O. Kanert, *Phys. Chem. Glasses* **33**, 109 (1992). (c) D. L. Sidebottom, P. F. Green, and R. K. Brow, *J. Non-Cryst. Solids* **203**, 300 (1995).

[105] P. Lunkenheimer and A. Loidl,in F. Kremer and A. Schönhals (eds), *Broadband Dielectric Spectroscopy*, Chapter 5, Springer, Berlin, 2002.

[106] P. Lunkenheimer, A. Pimenov, M. Dressel, B. Gorshunov, U. Schneider, B. Schiener, and A. Loidl, *ACS Symp. Ser.* **676**, 168 (1997).

[107] P. Lunkenheimer, *Glassy Dynamics*, Shaker, Aachen, 1999.

[108] P. Lunkenheimer, L. C. Pardo, M. Köhler, and A. Loidl, *Phys. Rev. E* **77**, 031506 (2008).

[109] V. K. Malinovsky and A. P. Sokolov, *Solid State Commun.* **57**, 757 (1986).

[110] P. Lunkenheimer and A. Loidl, *J. Non-Cryst. Solids* **352**, 4556 (2006).

[111] S. R. Elliott, *Physics of Amorphous Materials*, Longman Scientific & Technical, Harlow, 1990.

[112] V. G. Karpov, M. I. Klinger, and F. N. Ignatiev, *Sov. Phys. JETP* **57**, 439 (1983).

[113] U. Buchenau, Yu. M. Galperin, V. L. Gurevich, D. A. Parshin, M. A. Ramos, and H. R. Schober, *Phys. Rev. B* **46**, 2798 (1992).

[114] S. R. Elliott, *Europhys. Lett* **19**, 201 (1992).

[115] V. K. Malinovsky, V. N. Novikov, and A. P. Sokolov, *J. Non-Cryst. Solids* **90**, 485 (1987).

[116] W. Schirmacher, G. Diezemann, and C. Ganter, *Phys. Rev. Lett.* **81**, 136 (1998).

[117] W. Götze and M. R. Mayr, *Phys. Rev. E* **61**, 587 (2000).

[118] (a) R. Casalini and C. M. Roland, *J. Chem. Phys.* **119**, 11951 (2003). (b) R. Casalini and C. M. Roland, *Phys. Rev. Lett.* **91**, 015702 (2003). (c) S. Pawlus, S. Hensel-Bielowka, K. Grzybowska, J. Zioło, and M. Paluch, *Phys. Rev. B* **71**, 174107 (2005). (d) R. Casalini and C. M. Roland, *Phys. Rev. B* **69**, 094202 (2004). (e) K. Grzybowska, A. Grzybowski, S. Pawlus, S. Hensel-Bielowka, and M. Paluch, *J. Chem. Phys.* **123**, 204506 (2005). (f) K. Grzybowska, S. Pawlus, M. Mierzwa, M. Paluch, and K. L. Ngai, *J. Chem. Phys.* **125**, 144507 (2006). (g) T. Hayakawa and K. Adachi, *Polymers* **42** 1725 (2001).

[119] (a) M. Paluch, R. Casalini, S. Hensel-Bielowka, and C. M. Roland, *J. Chem. Phys.* **116**, 9839 (2002). (b) K. L. Ngai and M. Paluch, *J. Phys. Chem. B* **107**, 6865 (2003).

[120] A. Schönhals, F. Kremer, A. Hofmann, E. W. Fischer, and E. Schlosser, *Phys. Rev. Lett.* **70**, 3459 (1993).

[121] Additional uncertainty of τ_α(241K) arises from the fact that at that temperature the α-peak was outside the investigated frequency window (Fig. 3.6b) and an assumption on the peak height had to be made to arrive at a reasonable estimate of the relaxation time.

[122] L. C. Pardo, P. Lunkenheimer, and A. Loidl, *Phys. Rev. E* **76**, 030502(R) (2007).

[123] (a) N. B. Olsen, T. Christensen, and J. C. Dyre, *Phys. Rev. Lett* **86**, 1271 (2001). (b) A. Brodin, C. Gainaru, V. Porokhonskyy, and E. A. Rössler, *J. Phys. Condens. Matter* **19**, 205104 (2007).

[124] P. Lunkenheimer, U. Schneider, R. Brand, and A. Loidl, *AIP Conf. Proc.* **469**, 433 (1999).

[125] P. Lunkenheimer, R. Wehn, Th. Riegger, and A. Loidl, *J. Non-Cryst. Solids* **307–310**, 336 (2002).

[126] Here one should note that the justification for using a simple *additive* superposition of different contributions to $\varepsilon''(\nu)$ may be doubted and alternatives were promoted [82]. However, usually the convolution approach proposed, for example, in Ref. 82 leads to similar results [84, 108].

[127] T. Psurek, S. Maslanka, M. Paluch, R. Nozaki, and K. L. Ngai, *Phys. Rev. E* **70**, 011503 (2004).

[128] H. Yardimci and R. L. Leheny, *J. Chem. Phys.* **124**, 214503 (2006).

[129] (a) N. B. Olsen, *J. Non-Cryst. Solids* **235–237**, 399 (1998). (b) N. B. Olsen, T. Christensen, and J. C. Dyre, *Phys. Rev. E* **62**, 4435 (2000).

[130] D. Prevosto, S. Capaccioli, M. Lucchesi, P. A. Rolla, and K. L. Ngai, *J. Chem. Phys.* **120**, 4808 (2004).

[131] E. Kaminska, K. Kaminski, M. Paluch, and K. L. Ngai, *J. Chem. Phys.* **124**, 164511 (2006).

[132] (a) W. M. Du, G. Li, H. Z. Cummins, M. Fuchs, J. Toulouse, and L. A. Knauss, *Phys. Rev. E* **49**, 2192 (1994). (b) E. Rössler, V. N. Novikov, and A. P. Sokolov, *Phase Transit.* **63**, 201 (1997). (c) W. Götze, *J. Phys. Condens. Matter* **11**, A1 (1999).

[133] H. Z. Cummins, G. Li, Y. H. Hwang, G. Q. Shen, W. M. Du, J. Hernandez, and N. J. Tao, *Z. Phys.* **103**, 501 (1997).

[134] H. Z. Cummins, *J. Phys. Condens. Matter* **11**, A95 (1999).

[135] A. Yoshihara, H. Sato, and S. Kojima, *Prog. Theor. Suppl.* **126**, 423 (1996).

[136] A. Yoshihara, H. Sato, and S. Kojima, *Jpn. J. Appl. Phys.* **35**, 2925 (1996).

[137] A. Yoshihara, H. Sato, K. Takanashi, and S. Kojima, *Physica B* **219**, 273 (1996).

[138] (a) T. Franosch, W. Götze, M. R. Mayr, and A. P. Singh, *Phys. Rev. E* **55**, 3183 (1997). (b) W. Götze and T. Voigtmann, *Phys. Rev. E* **61**, 4133 (2000).

[139] P. Rösner, K. Samwer, and P. Lunkenheimer, *Europhys. Lett.* **68**, 226 (2004).

[140] R. Brand, P. Lunkenheimer, and A. Loidl, *J. Chem. Phys.* **116**, 10386 (2002).

[141] S. A. Kivelson and G. Tarjus, *Nat. Mater.* **7**, 831 (2008).